

2017-08-15

Ocean forcing of Ice Sheet retreat in central west Greenland from LGM to the early Holocene

Jennings, AE

<http://hdl.handle.net/10026.1/9591>

10.1016/j.epsl.2017.05.007

Earth and Planetary Science Letters

Elsevier BV

All content in PEARL is protected by copyright law. Author manuscripts are made available in accordance with publisher policies. Please cite only the published version using the details provided on the item record or document. In the absence of an open licence (e.g. Creative Commons), permissions for further reuse of content should be sought from the publisher or author.

1 **Ocean forcing of Ice Sheet Retreat in Central West Greenland from LGM through**
2 **Deglaciation**

3

4 Anne E. Jennings^{a*}, John T. Andrews^{a,b}, Colm Ó Cofaigh^c, Guillaume St. Onge^d,
5 Christina Sheldon^e, Simon T. Belt^f, Patricia Cabedo-Sanz^f, Claude Hillaire-Marcel^g

6

7 (a) INSTAAR, University of Colorado, Boulder, CO 80309, USA

8 (b) Department of Geological Sciences, University of Colorado, Boulder, CO, 80309,
9 USA

10 (c) Department of Geography, Durham University, Science Site, South Road, Durham,
11 DH1 3LE, UK

12 (d) Institut des sciences de la mer de Rimouski (ISMER) & GEOTOP, Université du
13 Québec à Rimouski, 310, allée des Ursulines, Rimouski, Québec, Canada, G5L 3A1

14 (e) Centre for Past Climate Studies and Arctic Research Centre, Department of
15 Geoscience, Aarhus University, Aarhus, Denmark

16 (f) Biogeochemistry Research Centre, School of Geography, Earth and Environmental
17 Sciences, Plymouth University, Drake Circus, Plymouth, PL4 8AA, UK

18 (g) GEOTOP-UQAM, Montreal, QC, Canada

19

20 * Corresponding author

21 INSTAAR

22 University of Colorado

23 Boulder, CO 80309-0450

24 USA

25 Anne.jennings@colorado.edu

26

27 Keywords: central west Greenland; Greenland Ice Sheet; Baffin Bay; LGM; foraminifera;
28 ocean forcing

29

30 **Abstract**

31 Three radiocarbon dated sediment cores from trough mouth fans on the central west
32 Greenland continental slope were studied to determine the timing and processes of
33 Greenland Ice Sheet (GIS) retreat from the shelf edge during the last deglaciation and to
34 test the role of ocean forcing (i.e. warm ocean water) thereon. Analyses of lithofacies,
35 quantitative x-ray diffraction mineralogy, benthic foraminiferal assemblages, the sea-ice
36 biomarker IP₂₅, and $\delta^{18}\text{O}$ of the planktonic foraminifera *Neogloboquadrina pachyderma*
37 sinistral from sediments in the interval from 17.5-10.8 cal ka BP provide consistent
38 evidence for ocean and ice sheet interactions during central west Greenland (CWG)
39 deglaciation. The Disko and Uummannaq ice streams both retreated from the shelf edge
40 after the last glacial maximum (LGM) under the influence of subsurface, warm Atlantic
41 Water. The warm subsurface water was limited to depths below the ice stream grounding
42 lines during the LGM, when the GIS terminated as a floating ice shelf in a sea-ice
43 covered Baffin Bay. The deeper Uummannaq ice stream retreated first, (ca. 17.1 cal ka
44 BP), while the shallower Disko ice stream retreated at ca. 16.2 cal ka BP. The grounding
45 lines were protected from accelerating mass loss (calving) by a buttressing ice shelf and
46 by landward shallowing bathymetry on the outer shelf. Calving retreat was delayed until
47 ca. 15.3 cal ka BP in the Uummannaq Trough and until 15.1 cal ka BP in the Disko
48 Trough, during another interval of ocean warming. Instabilities in the Laurentide,
49 Innuitian and Greenland ice sheets with outlets draining into northern Baffin Bay
50 periodically released cold, fresh water that enhanced sea ice formation and slowed GIS
51 melt. During the Younger Dryas, the CWG records document strong cooling, lack of GIS
52 meltwater, and an increase in iceberg rafted material from northern Baffin Bay. The ice
53 sheet remained in the cross-shelf troughs until the early Holocene, when it retreated

54 rapidly by calving and strong melting under the influence of atmosphere and ocean
55 warming and a steep reverse slope toward the deep fjords. We conclude that ocean
56 warming played an important role in the palaeo-retreat dynamics of the GIS during the
57 last deglaciation.

58

59 **1. Introduction**

60 Understanding the response of the Greenland Ice Sheet (GIS) to past large changes in
61 climate and ocean forcing provides scope to place the dramatic current changes (e.g.,
62 Bamber et al., 2012; Enderlin et al., 2014) into a longer time-perspective and provides
63 context for model predictions of future changes in the area and volume of the GIS.
64 Currently, the GIS is losing mass by surface melt, runoff and ice discharge from outlet
65 glaciers, with the total mass loss contributing to global sea level rise (Enderlin et al.,
66 2014), and likely impacting on the Atlantic Meridional Overturning Circulation (Bamber
67 et al., 2012). The GIS is complex, however, with many marine-terminating glaciers,
68 which have a range of flow rates that vary with time (Rignot and Mouginot, 2012; Moon
69 et al., 2012). Ocean forcing of grounding-line retreat has been documented in some of the
70 fastest flowing of Greenland’s outlet glaciers (e.g., Holland et al., 2008; Straneo et al.,
71 2012), but the processes are complex and responses by individual outlet glaciers vary (cf.
72 Joughin et al., 2012; Nick et al., 2009; Straneo and Heimbach, 2013; Rignot et al., 2015).
73 Although these modern observations are compelling, the short time-period over which
74 they span severely limits our ability to forecast GIS response to modern warming.

75 During the Last Glacial Maximum (LGM), the GIS advanced onto the continental
76 shelf but it had retreated behind its present margin by the middle Holocene (cf. Funder et

77 al., 2011; Larsen et al., 2015). Model reconstructions indicate an excess of ice equivalent
78 sea level that reached a maximum of 5.1 m at 16.5 cal ka BP (Lecavalier et al., 2014),
79 highlighting the large negative change in mass balance during deglaciation. Here, we
80 present multi-proxy sediment core data on three previously unpublished sediment cores
81 to reconstruct the LGM to Holocene GIS history of CWG, where some of the fastest
82 flowing calving glaciers of the modern ice sheet enter the sea (Rignot et al., 2012). The
83 cores are from the upper continental slope, beyond the maximum LGM extent of
84 grounded ice at the shelf edge (Ó Cofaigh et al., 2013a,b), thus allowing them to capture
85 a sediment record of the oceanographic and environmental conditions that preceded and
86 accompanied ice retreat. Importantly, such a perspective was lacking in earlier research
87 where the timing of ice retreat was estimated based on (i) radiocarbon dates from outer
88 shelf cores that record the timing of retreat already underway (Jennings et al., 2014;
89 Sheldon et al., 2016) and (ii) radiocarbon dates from shells entrained in sediment gravity
90 flows on the Disko trough mouth fan (TMF), which likely reflect remobilization of
91 sediments by a Younger Dryas re-advance of Jakobshavns Isbrae (Ó Cofaigh et al.,
92 2013b) rather than LGM ice activity. Building on this previous work, we address the
93 following specific questions: When did the ice margin retreat from the shelf edge and did
94 it retreat episodically, gradually or rapidly? Did ocean warming (Atlantic Water inflow)
95 initiate and sustain retreat? Finally, we consider how the major events of GIS mass
96 change recorded off CWG relate to the N. Hemisphere climate history recorded in the
97 Greenland ice cores. Combined, we develop a conceptual model of GIS ice retreat and
98 the drivers of retreat from the results of these analyses.
99

100 **2. Environmental Setting**

101 Large cross-shelf troughs formed by fast flowing ice streams of the GIS terminate
102 on the slope as major TMFs (Fig. 1) that accumulated during glacial-interglacial cycles
103 (Hofmann et al., 2016a). The Uummanaq TMF is dominated in its upper part by
104 glaciogenic debris flows, deposited when the Uummanaq ice stream was last at the shelf
105 edge during the LGM (Ó Cofaigh et al., 2013a; Dowdeswell et al., 2014). This cross-
106 shelf trough joins the slope at c. 600 m water depth in a wide reentrant on the outer shelf
107 (Fig. 1). By contrast, the Disko cross-shelf trough joins the slope at 350–400 m depth on
108 the south side of the Disko TMF.

109 The West Greenland Current (WGC) is the source for warm ocean water along
110 the western margin of the GIS, beginning where the East Greenland Current (EGC) and
111 the Irminger Current (IC) become confluent as they round the southern tip of Greenland
112 (Fig. 1). Cold, low salinity Polar Water originating in the EGC forms the surface layer
113 close to the coast and is augmented by glacier melt as it proceeds northward (Ribergaard
114 et al., 2008). Warmer, saline Atlantic Water originating in the IC flows below and west
115 of the Polar Water (Buch, 2000a, b) and, in Baffin Bay, forms the West Greenland
116 Intermediate Water (WGIW) that submerges beneath the Arctic Surface Water (ASW)
117 (Fig. 1) (Tang et al., 2004). These two components mix as they track northward along the
118 shelf and shelf break and can enter the inner shelf and fjords, affecting outlets of the GIS
119 grounded below sea level (Holland et al., 2008). The WGC is marked by lower sea-ice
120 concentration and thickness along west Greenland (Tang et al., 2004). ‘Vest-isen’, the
121 first-year ice formed in Baffin Bay (Buch et al., 2004), usually begins to form in
122 September, expands from north to south, and reaches a maximum extent in March. It

123 forms on the relatively fresh, cold ASW that enters from the Canadian Archipelago, and
124 occupies the upper 100–300 m of the water column (Fig. 1). A second source of sea ice,
125 the ‘Stor-isen’, travels into the area around SW Greenland with Polar Water of the EGC
126 (Buch et al., 2004).

127 The connection between Baffin Bay and the Arctic Ocean was blocked by
128 confluent Greenland, Innuitian and Laurentide ice sheets until the early Holocene
129 (England et al., 2006; Zreda et al., 1999; Jennings et al., 2011), thus preventing the flow
130 of ASW into Baffin Bay. Poor carbonate preservation in Baffin Bay by at least 5 cal ka
131 BP (cf. Andrews and Eberl, 2011) is attributed to the inflow of carbonate under-saturated
132 Arctic Surface Water (Azetsu-Scott et al., 2010) after deglaciation of the channels at the
133 head of Baffin Bay (Jennings et al., 2011). In contrast, calcareous faunas are well
134 preserved on the west Greenland Shelf under the influence of Atlantic water carried in the
135 WGC (eg Perner et al., 2012).

136

137 **3. Materials and Methods**

138 During two research cruises to Baffin Bay, we acquired sediment cores from the upper
139 parts of the Disko and Uummannaq TMFs. The cores investigated in the current study are
140 HU2008029-12PC (68°13.69' N; 57°37.08' W; 1475 m water depth), collected in 2008
141 from the Canadian vessel CSGS Hudson, together with JR175-VC29 (68°07.35' N;
142 59°44.36' W; 1064 m water depth) and JR175-VC46 (70°28.13' N; 61°2.91' W; 845 m
143 water depth) collected in 2009 from the UK vessel RRS James Clark Ross (Fig. 1).

144 Core chronologies are based on radiocarbon (^{14}C) dates on planktonic and benthic
145 foraminifera and molluscs (Fig. 2; Table 1). ^{14}C dates were calibrated using the

146 Marine13 curve (Reimer et al., 2013). OxCal version 4.2.4 (Ramsey and Lee, 2013) was
147 used to compute age/depth models and age uncertainties. We assume a marine reservoir
148 offset (ΔR) of 140 ± 30 years based on recent work in Disko Bugt (Lloyd et al., 2011) and
149 to align with recently published West Greenland core chronologies (cf Jennings et al.,
150 2014; Hogan et al., 2016; Sheldon et al., 2016). ΔR was likely larger in the LGM, but its
151 magnitude and variation through time are unknown. Simon et al. (2012) support a ΔR
152 range of 0–400 years in central Baffin Bay, which encompasses the ΔR value we have
153 used.

154 To reconstruct the timing and environmental conditions of ice retreat, we have
155 established basic lithofacies divisions for each core based on the sedimentary structures
156 seen in x-radiographs and x-ray computed tomography (CT) scans (Fig. 2). We
157 measured a series of climate/environmental proxies on each core and placed these into
158 the context of the lithofacies changes. Our proxy data include counts of >2 mm clasts
159 from x-radiographs (VC46 and VC29), and CT scans (12PC) of split cores as a measure
160 of variations in ice-rafted debris (IRD) (Grobe, 1987). High counts of IRD are
161 interpreted to reflect increased mass loss from the ice sheet by calving or as evidence of
162 enhanced iceberg melt.

163 We distinguished the relative proportions of two major sediment sources, ‘distal’
164 northern Baffin Bay and ‘local’ CWG, to the TMFs using statistical analysis of
165 quantitative x-ray diffraction mineralogy (qXRD) and the application of a sediment
166 unmixing model applied to mineralogical analysis of a suite of Baffin Bay surface
167 sediments (see Andrews and Eberl, 2011, 2012). Changes in sediment provenance
168 indicate whether hemipelagic sediments on the TMFs were supplied by ‘local’ Disko and

169 Uummannaq ice streams, and potentially sediments from other West Greenland outlets,
170 or by distal Laurentide, Innuitian and north GIS ice margins terminating in northern
171 Baffin Bay (NBB) (Li et al., 2011; England et al., 2006) (Fig. 1). The provenance data
172 are reported as sediment source fractions attributed to NBB vs. CWG (Supp. Fig. 1). The
173 mineralogy of the CWG ice streams is distinct from central Baffin Bay (Simon et al.,
174 2014) and the Davis Strait (Andrews et al., 2014). The most obvious signal of NBB
175 glacier margin input is detrital carbonate including dolomite and calcite eroded from
176 Paleozoic carbonate bedrock, and the NBB source as reconstructed herein is closely tied
177 to its occurrence (Andrews and Eberl, 2011) (Fig. 1; Supp. Fig. 1).

178 Benthic and planktonic foraminiferal assemblages were quantified and Principal
179 Component Analysis (PCA) of the benthic assemblages of each core was run separately,
180 providing a set of principal component axes for each core. Known environmental
181 associations of the most important benthic species on the PCA axes from each core were
182 then used to interpret changes in the presence of relatively warm Atlantic Water as a
183 subsurface water mass (AIW), glacial meltwater production, water-column stratification
184 with cold/sea-ice covered surface waters, and onset of the WGC at the core sites (Table 2;
185 Fig. 3).

186 Stable isotope data on the planktic foraminifer *Neogloboquadrina pachyderma*
187 sinistral (NPS) acquired from VC29 are used to test for isotopically light glacial
188 meltwater during deglaciation. The biomarker IP₂₅ (Belt et al., 2007) was quantified in
189 12PC only, to assess for the presence of seasonal sea ice. Descriptions of all proxy
190 methods are in the Supplemental Information.

191

192 **4. Background and previous work**

193 Evidence on the extent of the GIS at the LGM has grown in recent years but is still sparse
194 for many areas (Funder et al., 2011; Vasskog et al., 2015). Geophysical data collected in
195 2009 showed that grounded ice extended across the CWG margin through the
196 Uummannaq and Disko troughs as fast flowing ice streams (Ó Cofaigh et al., 2013a, b;
197 Dowdeswell et al., 2014). Debris flows and turbidites on the Disko and Uummannaq
198 TMFs also provide evidence for an ice sheet margin grounded at the shelf edge (Ó
199 Cofaigh et al., 2013a,b). A minimum estimate of the timing of ice retreat from the outer
200 Uummannaq trough is provided by a ^{14}C date of 15 cal ka BP in glacial marine sediments
201 overlying till on the shelf (Ó Cofaigh et al., 2013b; Sheldon et al., 2016). Sheldon et al.
202 (2016) proposed that a large grounding zone wedge in the outer-middle reaches of the
203 Uummannaq Trough marks a stable ice position during the Younger Dryas (YD) and that
204 the Uummannaq Ice Stream retreated episodically from its LGM shelf edge position.

205 The timing of LGM retreat from the Disko Trough shelf edge is not well
206 constrained due to a YD re-advance of the ice stream; however, an estimate of ice retreat
207 from the LGM position c. 13.8 cal ka BP is based on ^{14}C dates on shells entrained in
208 sediment gravity flows in cores from the Disko TMF (Ó Cofaigh et al., 2013b). New 3D-
209 seismic mapping of the banks adjacent to Disko Trough suggests that grounded ice
210 retreated in phases from the LGM position and that the GIS grounded ice on the middle
211 shelf banks during the YD (Hofman et al., 2016b). Hogan et al. (2016) showed that the
212 ice margin stabilized on an inner shelf bathymetric high c. 12.1 cal ka BP (Hogan et al.,
213 2016). YD ice retreat in CWG is marked by increased IRD flux (Jennings et al., 2014;

214 Sheldon et al., 2016) consistent with rapid ice retreat into the fjords (Lane et al., 2014;
215 Roberts et al., 2013; Hogan et al., 2011).

216 Knutz et al. (2011) proposed a model of ice retreat for southern Greenland in
217 which the initial retreat from the shelf edge was promoted by subsurface Atlantic Water
218 from the IC. The ensuing rapid mass loss by calving produced pulses of ice rafted clasts
219 (IRD) between the LGM and the early Holocene with predominantly Greenland
220 provenance signatures (Knutz et al., 2013). Offshore of CWG, the WGC was established
221 by 14 cal ka BP in association with strong melting of icebergs from Northern Baffin Bay
222 and West Greenland ice margins (Sheldon et al., 2016). NBB icebergs melted
223 preferentially along the CWG slope and outer shelf through contact with the warm WGC
224 thus forming a conspicuous detrital carbonate-rich layer, or DC event (Sheldon et al.,
225 2016), that is at least partly correlative with a marker of ice margin instability of northern
226 Baffin Bay ice streams, Baffin Bay Detrital Carbonate event 1 (BBDC1) (15-13.7 cal ka
227 BP) (Andrews et al., 1998; Simon et al., 2014). A younger BBDC event in the Disko
228 Trough from 11.6 to 10.6 cal ka BP (Jennings et al., 2014), correlates with the youngest
229 BBDC event in Baffin Bay (Simon et al., 2014) and with detrital carbonate events noted
230 on the Baffin Island shelf (Andrews et al., 1996) and central Davis Strait (Knutz et al.,
231 2013).

232

233 **5. Results presented on each core from North to South**

234 *5.1 JR175-VC46 (VC46), Uummannaq TMF*

235 The benthic foraminiferal faunal variations are summarized by the first 3 PC axes
236 (Figs. 3a, b; 4b, c, e; Supp. Info Table 1; Supp Fig. 2). VC46-PC1 explains 21.64% of the

237 variance in the assemblages. VC46-PC1 has positive scores on species found in
238 oligotrophic (*Stetsonia horvathi*) and pulsed productivity (*Islandiella helenae*) conditions
239 associated with sea-ice cover and AIW (*C. neoteretis*) (Fig. 3 A, B) (Jennings and
240 Helgadóttir, 1994; Wollenburg and Mackensen, 1998; Wollenburg et al., 2004) (Table 2).
241 Positive loadings on VC46-PC1 are interpreted to represent water-column stratification
242 with cold, sea-ice bearing surface waters with a warmer subsurface AIW layer.

243 VC46-PC2 explains 14.2% of the variance in VC46 assemblages and is positively
244 associated with *E. excavatum* f. *clavata*, an opportunistic species capable of withstanding
245 unstable environmental conditions and turbid glacial meltwater (cf. Hald and Korsun,
246 1997) (Table 2; Fig. 3A). Positive loadings on PC Axis 2 are associated with unstable
247 conditions and presence of turbid glacial meltwater (Fig. 3A).

248 VC46-PC3 explains 11.8% of the variance in VC46 assemblages. Axis 3 has
249 negative species scores on Atlantic Water indicator species including: *Melonis*
250 *barleeanus*, *Islandiella norcrossi*, *Saccammina difflugiformis* and *Reophax subfusiformis*
251 (Table 2). Significant positive species scores are on *Stainforthia feylingi*, an arctic
252 species indicative of cold, low salinity surface waters (Lloyd, 2006) and seasonal sea ice
253 formation (Seidenkrantz, 2013). Negative sample scores on VC46-PC3 were interpreted
254 to indicate the presence of relatively warm AIW, below, or at, the grounding line of the
255 glaciers (Fig. 3B).

256 The chronology of VC46 is constrained by 3 radiocarbon dates (Fig. 2A). One-
257 sigma errors on the downcore age estimates range between 80 and 240 yrs. Matrix-
258 supported, massive diamicton, interpreted as glacial debris flows (GDFs) by Ó
259 Cofaigh et al. (2013a) occur from the base of the core (558 cm) to 270 cm. The GDFs

260 record downslope sedimentation in front of the Uummannaq ice stream during the LGM
261 when it was grounded at the shelf edge (Ó Cofaigh et al., 2013a). GDF mineral
262 composition is dominated by the Greenland source but has a minor component from
263 northern Baffin Bay (Ó Cofaigh et al., 2013a) (Fig. 4A).

264 A unit of fine-grained bioturbated mud with a primarily West Greenland sediment
265 source and with rare or absent >2 mm clasts (IRD) overlies the GDFs from 270-180 cm
266 (17.1-15.3 cal ka BP) (Fig. 2A). A date on NPS from 262-267 cm constrains the timing
267 of the transition from GDFs into the overlying mud to 17.1 cal ka BP. At its top (198-
268 180 cm; 15.6-15.3 cal ka BP), the mud contains flame structures and a slight increase in
269 IRD suggesting rapid episodic deposition (Fig. 2A, Fig. 4A,E). The sediments in this
270 interval continue to be dominated by the Greenlandic source (0.8-1.0), although the NBB
271 source is present (up to 0.1) (Fig. 4A).

272 A transition to pebbly mud begins at 180 cm (15.3 cal ka BP) and extends to 115
273 cm (14 cal ka BP) (Fig. 2A). Within this, the IRD displays two large peaks (Fig. 4E).
274 The first peak, from 180-146 cm (15.3-14.7 cal ka BP) comprises sediments derived
275 primarily from CWG sources (Fig. 4A). The second peak, from 141-115 cm (14.5-14 cal
276 ka BP), contains a distinct rise in detrital carbonate from 14.3-14 cal ka BP (Fig. 4A, E)
277 indicative of an increased sediment contribution from northern Baffin Bay (Fig. 4A).
278 The NBB DC event is overlain by bioturbated mud with low IRD (Fig. 4E). A second
279 interval of pebbly mud from 85-25 cm is overlain by bioturbated mud. These units
280 postdate the uppermost radiocarbon age of 14.12 ± 0.08 cal ka BP at 120 cm (Fig. 2A).

281 The VC46 record begins with positive loadings on VC46-PC1 and 2 indicating
282 cold conditions associated with glacial meltwater and sea-ice cover between 17 and 16.9

283 cal ka BP, immediately after cessation of GDF deposition (Fig. 4C, D). A progressive,
284 warming signal is recorded by increasingly negative loadings on VC46-PC3 (16.9 to 16.2
285 cal ka BP) (Fig. 4B). This subsurface warm interval occurs within the bioturbated mud
286 overlying the GDFs. From 16.1 to 14.9 cal ka BP high positive loadings on VC46-PC2
287 indicate glacial meltwater in the upper part of the bioturbated mud and the lower unit of
288 pebbly mud (Fig. 4C). The meltwater signal declines after 14.9 cal ka BP, shortly before
289 the end of the IRD-rich pebbly mud with Greenlandic source (Fig. 4 A, C, E).

290 The upper IRD-rich interval between 14.5 and 14 cal ka BP is an NBB DC event
291 characterized by distinct shifts between VC46 PCA Axes 1 and 2, reflecting shifts in
292 cold, sea-ice covered conditions and glacial meltwater. The interval 14.5-14.0 cal ka BP
293 has positive VC46-PC1 loadings separated by a brief interval of positive loadings on
294 VC46-PC2 and strongly negative loadings on VC46-PC1. This pattern suggests that the
295 NBB DC event begins with a stratified water column, with cold, sea-ice covered waters
296 overlying submerged Atlantic Water (AIW) (14.5-14.3 cal ka BP). The environment
297 shifts briefly to relatively warmer conditions associated with glacial meltwater production
298 (14.3-14.2 cal ka BP) and then returns to cold sea surface with AIW conditions between
299 14.2 and 14 cal ka BP. The top of the dated record, coinciding with bioturbated mud,
300 shows a warming trend with increasing meltwater.

301

302 5.2 HU2008029-12PC (12PC) Northern Disko TMF

303 The first two PCA axes capture 44% of the variance in the benthic foraminiferal
304 assemblages (Fig. 3c). *S. feylingi* had significant positive scores on 12PC-PC1 (27.2% of
305 variance). This species is dominant under conditions of a cold freshwater lid and

306 associated sea-ice edge productivity (Seidenkrantz, 2013; Lloyd, 2006). The glacial
307 marine species *E. excavatum* and *C. reniforme* have negative scores on VC46-PC1. These
308 species are indicative of conditions warm enough to generate glacial meltwater.

309 12PC-PC2 (17.4% variance) is represented by negative scores of *M. barleeanus*,
310 *I. norcrossi*, *Buccella frigida* and *Nonionellina labradorica*. These species are consistent
311 with nutrient rich Atlantic Water. Negative sample scores on 12PC-PC2 are interpreted to
312 indicate the presence of AIW, below or at the grounding line of the glaciers, and thus
313 very similar to the VC46-PC3 (Fig. 3B, C).

314 Core 12PC extends well into the LGM, but for the purposes of comparison with
315 VC46 and VC29, we limit the discussion of data to ≤ 17.5 cal ka BP (554 cm). An age
316 reversal at 1 m limits the chronology to depths of ≥ 200 cm (11.9 cal ka BP). The 12PC
317 age model is based upon 5 radiocarbon dates from 201-691 cm on the arctic planktonic
318 foraminifer, NPS (Fig. 2B; Table 1). One-sigma errors on the downcore age estimates
319 are ± 100 years.

320 The CT number (CT#), a measure of sediment density, marks shifts in sand
321 content from high sand/high density to low sand/low density in the core (Fig. 5E). A
322 high CT# interval of bioturbated, stratified sand and mud from >17.5 cal ka BP (554 cm)
323 to 16.2 cal ka BP (467 cm) is overlain by much finer, crudely stratified mud with low
324 CT# that extends to 15.1 cal ka BP (356 cm) (Fig. 2B; Fig. 5E). The mud is dominated
325 by siliceous microfossils (centric diatoms and chaetoceras setae), and has rare IRD near
326 its base (Fig. 2B, Fig. 5D). The radiocarbon age from 469-470 cm closely constrains the
327 timing of the transition between these units to 16.2 ± 0.1 cal ka BP.

328 A prominent peak of negative 12PC-PC2 loadings begins prior to the transition
329 and ends soon after, indicating the presence of relatively warm ocean waters at
330 intermediate depths by 16.6 cal ka BP (Fig. 5C; Supplemental Figure 2). The presence of
331 the biomarker IP₂₅ indicates the occurrence of seasonal sea ice between 16.2 and 15.1 cal
332 ka BP (Fig. 5B), and the high diatom content of the sand fraction supports that this is also
333 an interval of increased marine productivity, although foraminifera were too sparse for
334 PCA analysis. Sand content, stratification and bioturbation increase at 15.1 cal ka BP
335 (356 cm) (Fig. 5E), coinciding with another peak from 15.1 to 14.9 cal ka BP in negative
336 loadings on 12PC-PC2 indicating warm subsurface water (Fig. 5C), but a fall in IP₂₅
337 content (Fig. 5B). At 14.3 cal ka BP (280 cm) coarse dispersed IRD and sand layers
338 become pronounced (Fig. 2B; Fig. 5D,E), coinciding with the shift from Greenland
339 sediment provenance to a mixed NBB (0.4) and Greenland (0.6) sediment provenance,
340 and marking an NBB DC event beginning at 14.3 cal ka BP (Fig. 5A). This transition is
341 preceded by a major rise in IP₂₅ (Fig. 5B) and a strongly negative 12PC-PC2 loading
342 (Fig. 5C), suggesting a shift to more consistent seasonal sea ice formation by 14.3 cal ka
343 BP.

344

345 5.3 JR175-VC29, Northern Disko TMF

346 The first three PCA axes explain 47.8% of the variance in the benthic
347 foraminiferal data (Fig. 3; Supp. Fig. 4). VC29-PC1 (19.4%) was associated with positive
348 scores on water column stratification indicators, *C. neoteretis* and *S. feylingi* and negative
349 scores on Atlantic Water indicators *Melonis barleeanus*, *B. frigida*, and *I. norcrossi* (Fig.
350 3D; Table 2). Negative loadings on VC29-PC1 are interpreted to express AIW similar to

351 VC46-PC3 and 12PC-PC2. VC29-PC2, accounting for 17.2 % of the variance separated
352 agglutinated from calcareous dominated assemblages and is not interpreted further.
353 VC29-PC3, accounting for 11.2 % of the variance, was associated with significant
354 positive scores of glacial marine species *E. excavatum* f. *clavata* reflecting Greenland
355 sourced turbid meltwater, as seen for VC46-PC2 and 12PC-PC2 (Fig. 3).

356 The VC29 chronology is based on 10 calibrated radiocarbon dates (Table 1;
357 Fig.2C) and spans the interval 15.9 to 10.8 cal ka BP. One-sigma errors on the downcore
358 age estimates range between 70 and 400 years (Fig. 2C).

359 Fine-grained, crudely stratified mud of Greenlandic provenance and rich in sand-
360 sized diatoms extends from 590 to 512 cm (15.9-15.1 cal ka BP) (Fig. 6A, Fig. 2C). This
361 unit has the highest negative loadings on VC29-PC1, indicating relatively warm
362 subsurface conditions, especially from 15.9 to 15.2 cal ka BP (Fig. 6B). NPS occurs in
363 high numbers (up to 200/g) coinciding with spikes in the benthic foraminiferal
364 abundances (Supp. Fig. 4) and records very light $\delta^{18}\text{O}$ values (2–0.7‰) indicating cold
365 low salinity surface water (Fig. 6C) or rapid sea ice formation (Hillaire-Marcel and de
366 Vernal, 2008). This unit is similar in timing and diatom content to the fine grained,
367 diatom-rich mud above the transition in 12PC (Fig. 5).

368 From 512-419 cm (15.1-14.0 cal ka BP) the sediments become sandy and well
369 stratified with progressively increasing IRD content, and ending with a pronounced
370 increase in IRD from 433-419 cm (14.2-14.0 cal ka BP) (Fig. 2C; Fig. 6E). By 15.1 cal
371 ka BP the loadings on VC29-PC1 trend toward positive values while loadings on VC29-
372 PC3 rise, suggesting increased glacial meltwater (Fig. 6B, D). This lithofacies has
373 Greenlandic provenance until the peak IRD interval (14.2-14 cal ka BP), which coincides

374 with a peak in NBB provenance up to 0.5 (Fig. 4A). PCA 1 becomes more positive
375 overall in this interval, recording ocean cooling, except for a peak from 14.4-14.2 cal ka
376 BP that records a brief reversal to warmer ocean conditions immediately prior to the
377 IRD/NBB peak (Fig. 6A, B). This negative peak in VC29-PC1 loadings is associated
378 with abundant *Cassidulina neoteretis* a species commonly associated with AIW around
379 Greenland (Table 2; Supp. Fig. 4) although absent in the >90% agglutinated faunas
380 (Sheldon, personal Communication) that occur today on the West Greenland slope due to
381 carbonate dissolution in Baffin Bay (Azetsu-Scott et al., 2010).

382 Between 419 and 282 cm (14-12.3 cal ka BP) there is a similar sequence of
383 lithofacies and provenance to the sequence below. The sequence begins with mud with
384 mixed NBB and Greenland provenance from 419-380 cm (14-13.6 cal ka BP). Between
385 380 and 334 cm (13.6-13 cal ka BP) the sediments change to stratified pebbly mud of
386 Greenlandic provenance (Fig. 6A, E). Steadily increasing loadings on VC29-PC1
387 indicate cooling (Fig. 6B). Positive loadings on VC29-PC3 change to negative loadings
388 by 13 cal ka BP indicating declining meltwater input (Fig. 6D). At 13 cal ka BP (334
389 cm) the NBB source returns abruptly and is associated with a rise in coarse IRD (Fig. 6A,
390 E). The NBB source continues to exceed the Greenland source until 12.3 cal ka BP. Over
391 the full period from 14-12.3 cal ka BP, VC29-PC1 trends gradually toward more positive
392 values indicating cooling ocean conditions (Fig. 6B) and planktic and benthic
393 foraminifera per gram are low, suggesting low productivity (Supp. Fig. 4).

394 Between 282 and 225 cm (12.3-11.6 cal ka BP) the sediments are sandy, crudely
395 stratified mud with rare IRD (Fig. 2C; Fig. 6E). This unit is dominated by the
396 Greenlandic source but maintains a background of 0.3 to 0.4 of NBB sediments (Fig.

397 6A). A shift to greater faunal abundances (Supp. Fig. 4) and more negative VC29-PC1
398 loadings supports slightly warmer conditions and a rise in VC29-PC3 loadings suggests
399 increased meltwater (Fig. 6B,D).

400 A final interval of stratified IRD rich sediment extends from 225-196 cm (11.6-
401 11.4 cal ka BP) (Fig. 2C; Fig. 6E). High IRD is once again associated with a pronounced
402 peak in NBB source up to 0.6 of the sediment (Fig. 6A). A dip in VC29-PC3 loadings
403 and very brief positive excursion in VC29-PC1 loadings support a brief cooling and
404 reduction in Greenlandic meltwater associated with this NBB/IRD peak (Fig. 6B, D).
405 The light stable isotope values on NPS (Fig. 6D) and strong rise in percentages of *S.*
406 *feylingi* (Supp. Fig. 5) indicate increased freshwater and icebergs from NBB.

407 Between 196 and 100 cm (11.4-10.9 cal ka BP) sediments are bioturbated sandy
408 mud with diminishing >2mm IRD (Fig. 2C; Fig. 6E). The NBB source declines (Fig. 6A)
409 and by 11 cal ka BP, VC29-PC1 shifts to higher/warmer values (Fig. 6B). Loadings on
410 VC29-PC3 increase steadily between 11.4 cal ka BP and 10.8 cal ka BP, indicating
411 increased meltwater (Fig. 6D). Above 100 cm (10.9 cal ka BP), the sediments transition
412 to bioturbated mud with rare IRD (Fig. 2C).

413

414 **6. Discussion**

415 We discuss our results via two questions that deal with the fundamental glaciological and
416 oceanographic changes in the location of the margin of the GIS in our study area.

417

418 *6.1 When did the GIS grounding line first retreat from the shelf edge and was its retreat*
419 *gradual, episodic or rapid?*

420 Using the stratigraphic relations, proxy data interpretations, and calibrated dates
421 of our three slope cores, we have built a conceptual model of grounding line retreat from
422 the shelf edge in CWG (Fig. 7). Our model is based on an earlier schematic model
423 (Knutz et al., 2011), but is developed further to reflect the new information on CWG
424 glacial history derived from our study. Two of the cores, VC46 and 12PC, have dated
425 sedimentary evidence marking Uummannaq and Disko ice stream retreat from the shelf
426 edge, respectively (Fig. 7A). In VC46, the end of GDF deposition and onset of
427 hemipelagic sedimentation at ca. 17.1 cal ka BP marks grounding-line retreat of the
428 Uummannaq ice stream. In 12PC, the strong reduction in sediment density at 16.2 cal ka
429 BP marks grounding-line retreat from the shelf edge of the Disko ice stream. In both
430 cores constraining ages are close to this boundary, supporting at least a 400 yr difference
431 (at 2- σ) in the timing of ice retreat between the Uummannaq and Disko ice streams. The
432 deeper shelf edge in Uummannaq Trough (>600 m) compared to the much shallower
433 shelf edge of the Disko Trough (350 to 400 m) may have allowed earlier access of warm
434 intermediate water to the Uummannaq ice stream grounding line, thereby assisting earlier
435 retreat.

436 In all three cores, a fine-grained interval essentially barren of IRD occurs after ice
437 retreat. The fine-grained unit extends to 15.1 cal ka BP in the case of the Disko TMF
438 cores (VC29 and 12PC) and to ca. 15.3 cal ka BP in the case of VC4 (age-equivalent at 1-
439 σ) (Figure 7B). Had the ice margins and grounding line retreated landward rapidly by
440 calving, this unit would have contained IRD clasts >2mm. Instead, we attribute the lack
441 of IRD to signify retention of a fringing ice shelf as the grounding line retreated slowly
442 across the outer shelf (Figure 7B). With an ice shelf, coarser-grained material would

443 have been preferentially deposited proximal to the grounding line, leaving icebergs
444 calved from the ice-shelf front relatively clean of debris (Domack and Harris, 1998).
445 Prior evidence for this scenario comes from geophysical data from the outer Uummannaq
446 trough where several small grounding zone wedges are defined on the landward
447 shallowing outer shelf (Sheldon et al., 2016; their Figure 2A), suggesting episodic retreat.
448 At the same time, fine sediments would have been carried to the slope sites in turbid
449 meltwater plumes emanating from the grounding line and by resuspension of fine
450 materials by currents (Fig. 7B), resulting in the fine grained mud unit (Domack and
451 Harris, 1998).

452 The rise in Greenlandic IRD by 15.3 cal ka BP in Uummannaq trough indicates
453 loss of the fringing ice shelf and retreat of a predominantly grounded ice front by calving
454 of debris-laden ice bergs (Figure 7C). In VC29 and 12PC, ice retreat by calving
455 commenced at 15.1 cal ka BP based on increasing sand content in 12PC and by the shift
456 to stratified sand with IRD in VC29. The age-control is best in VC29, suggesting that
457 15.1 cal ka BP is the better age estimate of the onset of the calving event (Fig. 2C),
458 although the rise in IRD is age-equivalent at 1- σ in the three cores. IRD may also have
459 been contributed by icebergs calved from outlet glaciers along the southwestern
460 Greenland margin.

461 In VC46 there is a clear end to the contribution of Greenland IRD by 14.7 cal ka
462 BP, with a lull in IRD contribution prior to the start of the second IRD peak at 14.5 cal ka
463 BP, and a peak in NBB sourced IRD from 14.3-14.0 cal ka BP. The NBB IRD event
464 began at 14.2 cal ka BP in VC29 and 12PC and ended by 14 cal ka BP; once again
465 overlapping 1- σ . In VC29 and 12PC, there is no distinct gap separating the Greenland

466 glacimarine sediments from the NBB IRD peak. An NBB event at 14 cal ka BP was also
467 observed in JR175-VC45 on the outer Uummannaq Trough (Sheldon et al., 2016). The
468 NBB West Greenland DC event essentially forms a marker horizon indicating an increase
469 in drift of NBB icebergs to the CWG margin where they melted preferentially as they
470 encountered warmer Atlantic Water. We infer that, prior to the early Holocene opening
471 of the channels in the Canadian Arctic Archipelago, the Baffin Current may have been
472 less vigorous, allowing Baffin Bay surface waters to spread within Baffin Bay such that
473 NBB icebergs could reach West Greenland.

474 A second phase of Greenland IRD and stratified sand began by 13.6 cal ka BP in
475 VC29 signifying renewed calving from the GIS, still grounded on the shelf. Once again,
476 this Greenland IRD interval is capped by IRD input from the NBB source at 13 cal ka
477 BP. The NBB event continued until 12.3 cal ka BP, when the provenance again became
478 dominated by Greenland sources. Between 12.3 and 11.6 cal ka BP, the Greenland
479 source was dominant and the sandy sediments likely record retreat of the Disko Ice
480 Stream from its Younger Dryas position at the shelf edge (Ó Cofaigh et al., 2013b;
481 Jennings et al., 2014). Between 11.6 and 11.4 cal ka BP there is a final NBB IRD event.
482 A DC event of similar onset but longer duration (11.6 to 10.6 cal ka BP) was recorded in
483 cores from the outer Disko Trough (Jennings et al., 2014). This final NBB event is
484 followed by deposition of dominantly Greenlandic sediment with coarse IRD and sand
485 that likely records ice retreat into Disko Bugt (Hogan et al., 2016), and, in Uummannaq
486 Trough, rapid retreat from the large mid-shelf grounding-zone wedge (Sheldon et al.,
487 2016;).

488 The results indicate that the GIS continued to contribute glaciogenic sediments
489 from iceberg rafting and meltwater plumes to the TMFs until the early Holocene. This
490 prolonged ice-stream sediment contribution to the fans supports other recent studies that
491 infer the presence of ice streams in the shelf troughs until the early Holocene (Hogan et
492 al., 2016; Sheldon et al., 2016). Our data also indicate that the ice sheet began to retreat
493 c. 17.1 cal ka BP in the Uummannaq Trough and at c. 16.2 cal ka BP in the Disko
494 Trough, coincident with gradual eustatic sea level rise associated with the main phase of
495 deglaciation (Lambeck et al., 2014). However, we do not know the exact change in
496 relative sea level (glacioisostatic and eustatic) and do not claim that sea-level rise was a
497 driver of ice retreat. The initial timing of grounding line retreat from the shelf edge along
498 CWG is therefore significantly earlier than 13.8 cal ka BP as inferred previously by Ó
499 Cofaigh et al., 2013b using data available at that time for the Disko ice stream, but older
500 than the 15 cal ka BP age of ice retreat from the Uummannaq ice stream recorded from
501 the outer Uummannaq trough (Sheldon et al., 2016; Dowdeswell et al., 2014). This key
502 outcome demonstrates that the initial CWG ice retreat from the shelf edge was closer in
503 timing to that of ice retreat in East Greenland of 18-17 cal ka BP, contrary to what was
504 previously thought (Vaskogg et al., 2015; Ó Cofaigh et al., 2013b; Jennings et al., 2006;
505 Evans et al., 2002).

506

507 *6.2 Did ocean warming (Atlantic Water inflow) initiate and sustain retreat?*

508 Our combined paleoceanographic proxy data provide consistent descriptions of the ocean
509 and sea ice conditions and ice-sheet/ocean interactions during deglaciation (Figure 8).
510 Furthermore, comparison of the proxy data with the GISP2 $\delta^{18}\text{O}$ record indicates how the

511 ice-sheet/ocean interactions that we document relate to the North Hemisphere climate
512 history recorded in the Greenland summit ice core climate record (Figure 8).

513 A parallel ocean-warming signal shown by the PC2 and PC3 in 12PC and VC46,
514 respectively, provides strong evidence that subsurface ocean warming preceded (12PC)
515 and accompanied ice retreat from the shelf edge. In both cores, the ocean-warming signal
516 rose sharply by 17 cal ka BP and reached a peak at 16.2 cal ka BP (Fig. 8D, I). Increased
517 productivity in 12PC prior to initial grounding line retreat is consistent with moderate
518 opening in sea-ice cover (Supp. Fig. 3; Fig. 5B; 7B). The timing of the ocean-warming
519 event coincides with, or slightly lags, Heinrich event 1 (c. 16.8 cal ka BP) from Hudson
520 Strait (Hemming, 2004). Warm subsurface water during stadials and Heinrich events has
521 been documented in the Nordic (Ezat et al., 2014) and Labrador seas (Marcott et al.,
522 2011). Knutz et al. (2011) reported warm SSTs between 16.8 and 16.4 cal ka BP from
523 southeastern Davis Strait reflecting IC advection (Fig. 8) that could also supply the warm
524 subsurface water farther north along the CWG margin.

525 Ocean warming continued after 16.2 cal ka BP, with a second subsurface ocean-
526 warming interval between 15.8 and 14.9 cal ka BP enveloping an IC advection event in
527 SE Davis Strait (Knutz et al., 2011) (Fig. 8). This interval encompasses the transition
528 from fine mud representing deposition in front of an ice shelf and pebbly mud reflecting
529 the onset of calving retreat of the Disko and Uummannaq ice streams. In VC29, the peak
530 warming between 15.4 and 15.2 cal ka BP (Fig. 8F) marks the end of strong ocean
531 stratification and in-situ sea ice formation shown by the very light stable isotopic values
532 in the planktic foraminifers (Fig. 6C) and the beginning of glacial meltwater fauna (Fig.
533 8F). The first calving retreat of the CWG grounding line followed Heinrich Event 1 and

534 is somewhat later than initial grounding line retreat defined for the southern GIS margin
535 (Knutz et al., 2011; 2013).. If the 15.1 cal ka BP calving is correlative with the Bølling
536 interstadial it would require shifting the calibrated ages by 400 years, suggesting the need
537 for a larger local reservoir correction (Fig. 8B).

538 A third warm peak is captured immediately before (VC29; Fig. 8F) and after
539 (12PC; Fig. 8D) the first NBB DC event between 14.3 and 14.0 cal ka BP. This marks
540 the end of the period of meltwater fauna associated with calving retreat of the Disko ice
541 stream (Fig. 8F), the entry of chilled Atlantic Water species, *C. neoteretis*, into the
542 benthic fauna (Supp. Fig. 3), and the beginning of consistent seasonal sea-ice occurrence
543 (Fig. 5B). In VC46, a brief interval of warming and meltwater fauna occurs within the
544 NBB DC event (Fig. 8A) and coincides with the MWP-1A (meltwater pulse 1A) from
545 14.5 to 14 cal ka BP (Lambeck et al., 2014). Together, these points signal the beginning
546 of WGC and a seasonal sea-ice edge in Baffin Bay between 14.4 and 14.0 cal ka BP (Fig.
547 8). The first NBB DC event off CWG from 14.3 to 14.0 cal ka BP overlaps with BBDC
548 1 defined as 15.0–13.7 cal ka BP (Simon et al., 2014), and definitively lags Heinrich
549 Event 1 (Andrews et al., 1998).

550 Ocean cooling and absence of a glacial meltwater fauna marks the NBB DC events
551 from 14.2 cal ka BP onwards in VC29 (Figure 8). In the three NBB DC intervals on West
552 Greenland (14.3 to 14.0, 13.0 to 12.3, and 11.6 to 11.4 cal ka BP), IRD counts are high
553 and meltwater fauna absent. Apart from 11.6–11.4 cal ka BP, these cold ocean periods
554 coincide with cool periods in the GISP 2 ice core record (Fig. 8A), including the Older
555 Dryas (GI-1d) and the Younger Dryas (GS-1) (Fig. 8). During the last two NBB DC
556 events, *S. feylingi* is the dominant species, consistent with seasonal sea-ice formation

557 (Seidenkrantz, 2013) off CWG, formed on NBB sourced freshwater (Supp. Fig. 5). The 3
558 intervals between the NBB DC events mark phases of CWG meltwater fauna and glacial
559 marine sediment input (Fig. 8), suggesting that absence of the NBB meltwater input
560 allows warming and melting of the GIS to prevail. In contrast, the presence of the cold
561 freshwater from NBB appears to have dampened GIS melting and retreat.

562

563 **7. Conclusions**

564 We interpret multi-proxy sediment data to propose that CWG ice streams
565 retreated from the shelf edge under the influence of subsurface, warm Atlantic Water that
566 resided initially at depths below the ice sheet grounding lines (Fig. 7A). Ice retreat
567 occurred either coincident with or shortly after Heinrich event 1. The deeper,
568 Uummannaq ice stream, retreated first, while retreat of the Disko ice stream from the
569 shelf edge was delayed until ca. 16.2 cal ka BP. Initial ice stream retreat did not produce
570 IRD. We suggest that ice stream flow was buttressed by the presence of a fringing ice
571 shelf, pervasive sea ice, and the level or normal (landward shallowing) bathymetry of the
572 outer shelf. We do not explain the atmospheric or ocean circulation forcing that caused
573 the subsurface warm ocean water to impinge on the grounding lines, but note that
574 advection of warm IC water was observed at similar times upstream of the CWG cores,
575 and that major changes in sea-surface conditions associated with Heinrich Event 1 may
576 have played a role. Large-scale calving retreat was delayed until c. 15.1 cal ka BP, or
577 slightly earlier in the Uummannaq system (15.3 cal ka BP), during a second interval of
578 subsurface ocean warming.

579 Northern Baffin Bay ice sheet margins released several intervals of cold, fresh
580 water and IRD during deglaciation. The freshwater release enhanced sea-ice formation
581 and slowed melting and GIS retreat. This is especially apparent in the formation of a
582 large grounding zone wedge in the Uummannaq Trough prior to, and during, the Younger
583 Dryas (12.8-11.6 cal ka BP) (Sheldon et al., 2016; Dowdeswell et al., 2014). At this
584 time, the CWG records document strong cooling, lack of GIS meltwater, and an increase
585 in IRD from northern Baffin Bay.

586 The GIS remained grounded in the cross-shelf troughs until the early Holocene,
587 when it retreated rapidly by calving and strong melting under the influence of atmosphere
588 and ocean warming and a reverse bed slope into the adjoining bays and the deep fjords.

589

590 **8. Acknowledgements:**

591 Funding for this research was provided by the US National Science Foundation grant
592 ARC1203492 and the UK Natural Environment Research Council grant NE/D001951/1.
593 We thank the officers crew and scientists aboard the RRS James Clark Ross during cruise
594 JR175 to West Greenland in 2009 and the technical expertise of British Geological
595 Survey personnel in core collection. We thank the captain, crew and scientists aboard the
596 2008 CSS Hudson cruise HU2008-029 for acquisition of core 2009029-12PC. We
597 gratefully acknowledge the microscope and x-ray diffraction research by undergraduate
598 research assistants, Brian Shreve, Jennifer Kelly, Matthew Reed, Kelly Cox and Matthew
599 Glasset. We gratefully acknowledge the helpful critique provided by 3 anonymous
600 reviewers.

601

602 **9. Figure Captions:**

603 Figure 1. Bathymetric map centered on Baffin Bay (BB) showing the locations of cores
604 studied and mentioned in the text. Radiocarbon dates from cores JR175-VC45, -VC35,
605 and -VC34 were used in previous studies to constrain the timing of GIS retreat from the
606 shelf edge (Ó Cofaigh et al., 2013a, b). The distribution of Paleozoic carbonate bedrock,
607 mapped ice margin positions in northern Baffin Bay (Li et al., 2011) and central West
608 Greenland (Ó Cofaigh et al., 2013a) and major ice streams are shown. UIS =
609 Uummannaq ice stream; DIS = Disko ice stream; SSIS = Smith Sound ice stream; LSIS =
610 Lancaster Sound ice stream. Northward-flowing West Greenland Current (WGC) is
611 shown by the thin red line and the southward flowing Baffin Current (BC) is shown as a
612 thin blue line. Inset shows temperature and salinity profile, 2008029-011CTD at the site
613 of 2008029-12PC.

614 [http://geoscan.nrcan.gc.ca/starweb/geoscan/servlet.starweb?path=geoscan/download.e](http://geoscan.nrcan.gc.ca/starweb/geoscan/servlet.starweb?path=geoscan/download.e&search1=R=261330)
615 [b&search1=R=261330](http://geoscan.nrcan.gc.ca/starweb/geoscan/servlet.starweb?path=geoscan/download.e&search1=R=261330).

616

617 Figure 2. Lithological logs against age-depth models for the three cores of this study.
618 Dark blue and light blue shading denote 1σ and 2σ uncertainties of the model in each
619 core. A. JR175-VC46. We exclude the upper 1 m from our age-depth model because the
620 upper part of the core is undated. B. 2008-29-12PC. Note that benthic foraminiferal ages
621 (green distributions) are not included in the age model; outliers at 1 m are excluded. C.
622 JR175-VC29. The upper 55 cm of data are excluded because it is undated. Modeled age
623 distributions are plotted for each dated sample (Table 1).

624

625 Figure 3. PCA scores of significant species on PCA axes of the 3 cores and their
626 environmental interpretations. A and B: JR175-VC46 species scores on the first 3 PCA
627 axes. C: 2008029-12PC, species scores on PCA axes 1 and 2. D: JR175-VC29 species
628 scores on PCA axes 1 and 3. See Supplemental Table 1 for full list of species scores.

629

630 Figure 4. Proxy data and lithofacies against calibrated age from JR175-VC46,
631 Uummannaq trough mouth fan. A. proportion of sediment from northern Baffin Bay
632 (brown) and the CWG (green). B, C, D. Foraminiferal PCA loadings on axes 1, 2, 3,
633 respectively. E. counts of >2mm grains attributed to iceberg rafting. Triangles on the x-
634 axis show locations of radiocarbon dates. Lithofacies: BM=bioturbated mud; FS=flame
635 structures; DMM=matrix supported diamicton.

636

637 Figure 5. Proxy data and lithofacies against calibrated age from 2008029-12 PC,
638 northern Disko trough mouth fan. A. proportion of sediment from northern Baffin Bay
639 (brown) and central West Greenland (green). B. IP₂₅ data. C. sample loadings on PCA
640 axis 2 where higher negative loadings indicate increased submerged Atlantic Water
641 influence. D. counts of >2mm clasts from the CT images. E. CT number and the
642 positions of radiocarbon ages that constrain this part of the chronology (black
643 arrowheads). Lithofacies: Strat Sndy Md=stratified sandy mud; Strat Sd/Md=Stratified
644 sand and mud.

645

646 Figure 6. Proxy data and lithofacies against calibrated age from JR175-VC29, northern
647 Disko trough mouth fan. A. proportion of sediment from northern Baffin Bay (brown)

648 and central West Greenland (green). B. foraminiferal PCA loadings on axes 1. C. $\delta^{18}\text{O}$
649 values from *Neogloboquadrina pachyderma* sinistral. D. foraminiferal PCA loadings on
650 axis 3. E. counts of >2mm grains attributed to iceberg rafting. Triangles on the x-axis
651 show locations of radiocarbon dates. Lithofacies: PMd=Pebbly mud; Strat Pb
652 Md=stratified pebbly mud.

653

654 Figure 7. Schematic illustrations summarizing the ice sheet ocean interactions in central
655 west Greenland (modified from Knutz et al., 2011). Panel A illustrates the LGM position
656 of the GIS outlets at the shelf edge with the ice margin feeding the trough mouth fans and
657 heavy sea ice in Baffin Bay. Panel B illustrates the initial retreat of the ice from the shelf
658 edge and retention of a buttressing ice shelf that filtered out coarse material at the
659 grounding line, released fines to the slope, and produced small grounding zone wedges
660 on the outer Uummannaq Trough. A slight reduction in buttressing sea ice is depicted.
661 Panel C illustrates the calving retreat of the ice sheet as the grounding line retreat toward
662 a reverse slope under the influence of warm ocean water. Red vertical bar denotes
663 location of the 3 cores in the study. Brown-based icebergs and IRD denote a northern
664 Baffin Bay (NBB) source whereas black-based icebergs denote a central West Greenland
665 (CWG) source. The onset of a seasonal sea ice presence is depicted.

666

667 Figure 8. Summary figure comparing key proxy records from VC46, VC29 and 12PC of
668 iceberg rafting (C, E, G), ocean warming and cooling (D, F, I), meltwater (blue horizontal
669 bars) and sediment provenance (gray bars) with GISP2 ice core $\delta^{18}\text{O}$ record (A) (Grootes
670 et al., 1993), eustatic sea level (B) (Lambeck et al., 2014) and the interpreted timing of

671 grounding line retreat, formation of the ice shelf, and calving retreat on the central West
672 Greenland margin. Red stars indicate peaks of ocean warming. Red arrows indicate
673 timing of IC advection events in core DA04-31P (Knutz et al., 2011). BBDC0 and
674 BBDC1 timing from Simon et al., 2014.

675

676 Table 1. Details concerning the radiocarbon dates from the 3 cores of this study and their
677 calibrated one sigma ranges, means and standard deviations as well as median values.

678 Brown highlighted rows show ages excluded from the age models.

679

680 Table 2. Benthic foraminiferal environmental preferences.

681

682 **10. References Cited**

683

684 Andrews, J.T., Eberl, D.D., 2011. Surface (sea floor) and near-surface (box cores)
685 sediment mineralogy in Baffin Bay as a key to sediment provenance and ice sheet
686 variations. *Can. J. Earth Sci.* 48 (9), 1307 - 1328. <http://dx.doi.org/10.1139/-11-021>.

687

688 Andrews, J.T., Eberl, D.D., 2012. Determination of sediment provenance by unmixing
689 the mineralogy of source-area sediments: The "SedUnMix" program. *Marine Geology*
690 291, 24-33.

691

692 Andrews, J.T., Gibb, O.T., Jennings, A.E., Simon, Q., 2014. Variations in the provenance
693 of sediment from ice sheets surrounding Baffin Bay during MIS 2 and 3 and export to the

694 Labrador Shelf Sea: site HU2008029-0008 Davis Strait. *Journal of Quaternary Science*
695 29, 3-13.
696
697 Andrews, J.T., Kirby, M.E., Aksu, A., Barber, D.C., Meese, D., 1998. Late quaternary
698 detrital carbonate (DC-) layers in baffin Bay Marine sediments (67°-74°N):
699 correlation with heinrich events in the North Atlantic? *Quaternary Science Reievs* 17,
700 125-1137. [http://dx.doi.org/10.1016/S0277-3791\(97\)00064-4](http://dx.doi.org/10.1016/S0277-3791(97)00064-4).
701
702 Andrews, J.T., Osterman, L.E., Jennings, A.E., Syvitski, J.P.M., Miller, G.H., Weiner,
703 N., 1996. Abrupt changes in marine conditions, Sunneshine Fiord, eastern Baffin Island,
704 N.W.T. (ca. 66° N) during the last deglacial transition: Links to the Younger Dryas cold-
705 event and Heinrich, H-0, in: Andrews, J.T., Austin, W., Bergsten, H., Jennings, H.E.
706 (Eds.), *Late Quaternary Paleoceanography of North Atlantic Margins*. Geological Society
707 of London, London, pp. 11-27.
708
709 Azetsu-Scott, K., Clarke, A., Falkner, K., Hamilton, J., Jones, P.E., Lee, C., Petrie, B.,
710 Prinsenber, S., Starr, M., Yeats, P., 2010. *Journal of Geophysical Research* 115,
711 C11021, doi:10.1029/2009JC005917.
712
713 Bamber, J.M. vanden Broeke, J. Ettema, J. Lenaerts, E. Rignot, E., 2012. Recent large
714 increases in freshwater fluxes from Greenland into the North Atlantic, *Geophysical*
715 *Research Letters* 39, L19501, doi:[10.1029/2012GL052552](http://dx.doi.org/10.1029/2012GL052552).
716

- 717 Belt, S.T., Massé, G., Rowland, S.J., Poulin, M., Michel, C., LeBlanc, B., 2007. A novel
718 chemical fossil of palaeo sea ice: IP₂₅. *Organic Geochemistry* 38, 16-27.
719
- 720 Buch E., 2000a. A monograph on the physical oceanography of the Greenland waters.
721 Danish Meteorological Institute Scientific Report, 00-12.
722
- 723 Buch E., 2000b. Air-sea-ice conditions off southwest Greenland, 1981–1997. *Journal of*
724 *Northwest Atlantic Fisheries Science* 26, 1–14.
725
- 726 Buch E., Pedersen S.A., Ribergaard M.H., 2004. Ecosystem variability in West
727 Greenland Waters. *E:journal of Northwest Atlantic Fishery Science* 34, part 2: 13–28.
728
- 729 Caralp, M. H., 1989. Size and morphology of the benthic foraminifer *Melonis*
730 *barleeanum*: Relationships with marine organic matter. *Journal of Foraminiferal*
731 *Research* 19, 235–245.
732
- 733 Corliss, B.H., 1991. Morphology and microhabitat preferences of benthic
734 foraminifera from the northwest Atlantic Ocean. *Marine Micropaleontology* 17, 195–236.
735
- 736 Domack, E.W., Harris, P.T., 1998. A new depositional model for ice shelves, based upon
737 sediment cores from the Ross Sea and the Mac. Roberson shelf, Antarctica. *Annals of*
738 *Glaciology* 27, 281-284.
739

- 740 Dowdeswell, J.A., Hogan, K.A., Ó Cofaigh, C., Fugelli, E.M.G., Evans, J., Noormets, R.,
741 2014. Late Quaternary ice flow in a West Greenland fjord and cross-shelf trough system:
742 submarine landforms from Rink Isbrae to Uummannaq shelf and slope. *Quaternary*
743 *Science Reviews* 92, 292-309. <http://dx.doi.org/10.1016/j.quascirev.2013.09.007>.
744
- 745 Enderlin, E. M., Howat, I.M., Jeong, S., Noh, M.-J., van Angelen, J. H., van den Broeke,
746 M.R., 2014. An improved mass budget for the Greenland ice sheet. *Geophysical*
747 *Research Letters* 41, 866–872, doi:10.1002/2013GL059010.
748
- 749 England, J., Atkinson, N., Bednarski, J., Dyke, A.S., Hodgson, D.A., Ó Cofaigh, C. 2006.
750 The Innuitian Ice Sheet: configuration, dynamics and chronology. *Quaternary*
751 *Science Reviews* 25, 689-703.
752
- 753 Evans, J., Dowdeswell, J.A., Grobe, H., Niessen, F., Stein, R., Hubberten, H.-W.,
754 Whittington, R.J., 2002. Late Quaternary sedimentation in Kejsers Franz Joseph Fjord and
755 the continental margin of East Greenland, in Dowdeswell, J.A., Ó Cofaigh, C., eds.,
756 *Glacier-Influenced Sedimentation on High-Latitude Continental Margins: Geological*
757 *Society of London Special Publication* 203, p. 149–179,
758 doi:10.1144/GSL.SP.2002.203.01.09.
759
- 760 Ezat, M.M., Rasmussen, T.L., Groeneveld, J., 2014. Persistent intermediate water
761 warming during cold stadials in the southeastern Nordic Seas during the past 65 k.y.
762 *Geology* 42, 663-666, doi: 10.1130/G35579.1.

763

764 Funder S., Kjeldsen K.K., Kjaer K., Ó Cofaigh C., 2011. The Greenland Ice Sheet During
765 the Past 300,000 Years: A Review. In: Ehlers J, Gibbard PL and Hughes PD (eds)
766 *Developments in Quaternary Sciences*. Amsterdam, The Netherlands: Elsevier, 699–713.

767

768 Grobe, H., 1987. A simple method for the determination of ice-rafted debris in sediment
769 cores. *Polarforschung* 57 (3), 123-126.

770

771 Grootes, P. M., Stuiver, M., White, J. W. C., Johnsen, S., Jouzel, J., 1993. Comparison of
772 oxygen isotope records from the GISP2 and GRIP Greenland ice cores. *Nature* 366, 552–
773 554.

774

775 Hald, M., Korsun, S. 1997. Distribution of modern benthic foraminifera from fjords of
776 Svalbard, European Arctic. *Journal of Foraminiferal Research* 27, 101–122.

777

778 Hemming, S.R., 2004. Heinrich events: massive late Pleistocene detritus layers of
779 the North Atlantic and their global climate imprint. *Reviews of Geophysics* 42, RG1005.

780

781 Hillaire-Marcel, C., deVernal, A., 2008. Stable isotope clue to episodic sea ice formation
782 in the glacial North Atlantic. *Earth and Planetary Science Letters* 268, 143–150.

783

- 784 Hofmann, J.C., Knutz, P.C., Nielsen, T., Kuijpers, A., 2016a. Seismic architecture and
785 evolution of the Disko Bay trough-mouth fan, central West Greenland margin,
786 *Quaternary Science Reviews*, <http://dx.doi.org/10.1016/j.quascirev.2016.05.019>
787
- 788 Hofmann, J.C., Knutz, P., Ó Cofaigh, C., 2016b. 3D-seismic observations of Late
789 Pleistocene glacial dynamics on the central West Greenland margin. EGU2016-15778.
790
- 791 Hogan, K.A., Dix, J.K., Lloyd, J.M., Long, A.J., Cotterill, C.J., 2011. Seismic
792 stratigraphy records the deglacial history of Jakobshavn Isbræ, West Greenland. *Journal*
793 *of Quaternary Science* 26, 757-766.
794
- 795 Hogan, K.A., Ó Cofaigh, C., Jennings, A.E., Dowdeswell, J.A., Hiemstra, J.F., 2016.
796 Deglaciation of a major palaeo-ice stream in Disko Trough, West Greenland. *Quaternary*
797 *Science Reviews*, <http://dx.doi.org/10.1016/j.quascirev.2016.01.018>
798
- 799 Höglund H., 1947. Foraminifera in the Gullmar Fjord and the Skagerrak. *Zoologiska*
800 *bidrag från Uppsala* 26, 3-328.
801
- 802 Holland, D.M., Thomas, R.H., de Young, B., Ribergaard, M.H., Lyberth, B., 2008.
803 Acceleration of Jakobshavn Isbræ triggered by warm subsurface oceanwaters. *Nature*
804 *Geoscience* 1 (10), 659e664. <http://dx.doi.org/10.1038/ngeo316>.
805

806 Jennings, A.E., Hald, M., Smith, L.M., and Andrews, J.T., 2006. Freshwater forcing from
807 the Greenland Ice Sheet during the Younger Dryas: Evidence from southeastern
808 Greenland shelf cores: *Quaternary Science Reviews* 25, 282–298,
809 doi:10.1016/j.quascirev.2005.04.006.

810

811 Jennings, A.E., Helgadottir, G., 1994. Foraminiferal assemblages from the fjords and
812 shelf of eastern Greenland. *Journal of Foraminiferal Research* 24 (2), 123e144.
813 <http://dx.doi.org/10.2113/gsjfr.24.2.123>.

814

815 Jennings, A.E., Sheldon, C., Cronin, T.M., Francus, F., Stoner, J, Andrews, J., 2011. The
816 Holocene history of Nares Strait, transition from glacial bay to Arctic-Atlantic
817 throughflow. *Oceanography* 24, no. 3, 26-41.

818

819 Jennings, A.E., Walton, M.E., Cofaigh, C.Ó., Kilfeather, A., Andrews, J.T., Ortiz, J.D., et
820 al., 2014. Paleoenvironments during Younger Dryas-early Holocene retreat of the
821 Greenland ice sheet from outer Disko Trough, central west Greenland. *Journal of*
822 *Quaternary Science* 29 (1), 27-40. <http://dx.doi.org/10.1002/jqs.2652>.

823

824 Jennings, A.E., Weiner, N.J., Helgadottir, G., Andrews, J.T., 2004. Modern foraminiferal
825 faunas of the southwestern to northern Iceland shelf: oceanographic and environmental
826 controls. *Journal of Foraminiferal Research* 34, 180-207.

827

- 828 Joughin, I., Alley, R. B., Holland, 2012. D. M. Ice-sheet response to oceanic forcing.
829 *Science* 338, 1172–1176.
830
- 831 Knudsen, K. L., Seidenkrantz, M.-S. 1994. *Stainforthia feylingi* new species from arctic
832 to subarctic environments, previously recorded as *Stainforthia schreibersiana* (Czjzek).
833 Cushman Foundation for Foraminiferal Research, Special Publication 32, 5–13.
834
- 835 Knutz, P. C., Sicre, M.-A., Ebbesen, H., Christiansen, S., Kuijpers, A., 2011.
836 Multiple- stage deglacial retreat of the southern Greenland Ice Sheet linked with Irminger
837 Current warm water transport, *Paleoceanography* 26, PA3204,
838 doi:10.1029/2010PA002053.
839
- 840 Knutz, P.C., Storey, M., Kuijpers, A., 2013. Greenland iceberg emissions constrained by
841 $^{40}\text{Ar}/^{39}\text{Ar}$ hornblende ages: Implications for ocean-climate variability during last
842 deglaciation. *Earth and Planetary Science Letters*, doi:10.1016/j.epsl.2013.06.008.
843
- 844 Korsun, S., Polyak, L. 1989. Distribution of benthic foraminiferal morphogroups in the
845 Barents Sea. *Oceanology* (Russia) 29, 838–844 (English translation).
846
- 847 Lambeck, K., Rouby, H., Purcell, A., Sun, Y., Sambridge, M., 2014. Sea level and global
848 ice volumes from the Last Glacial Maximum to the Holocene. *Proceedings of the*
849 *National Academy of Sciences of the United States of America* 111, 15296-15303.
850

- 851 Lane, T.P., Roberts, D.H., Rea, B.R., Ó Cofaigh, C., Vieli, A., Rodés, A., 2014. Controls
852 upon the last glacial maximum deglaciation of the northern Uummannaq ice stream
853 system, west Greenland. *Quaternary Science Reviews* 92, 324-344.
854 <http://dx.doi.org/10.1016/j.quascirev.2013.09.013>.
- 855
- 856 Larsen, N.K., Lecavalier, B., Bjørk, A.A., Colding, S., Huybrechts, P., Jakobsen, K.E.,
857 Kjeldsen, K.K., Knudsen, K.-L., Odgaard, B.V., Olsen, J., 2015. The response of the
858 southern Greenland ice sheet to the Holocene thermal maximum. *Geology* 43, 4, 291-294
859 doi:10.1130/G36476.1
- 860
- 861 Lecavalier, B.S., Milne, G.A., Simpson, M.J.R., Wake, L., Huybrechts, P., Tarasov, L.,
862 Kjeldsen, K.K., Funder, S., Long, A.J., Woodroffe, S., Dyke, A.S., Larsen, N., 2014. A
863 model of Greenland ice sheet deglaciation constrained by observations of relative sea
864 level and ice extent. *Quaternary Science Reviews* 102, 54-84.
- 865
- 866 Li, G., Piper, D.J.W., Campbell, D.C., 2011. The Quaternary Lancaster Sound trough-
867 mouth fan, NW Baffin Bay. *Journal of Quaternary Science* 26, 511–522.
- 868
- 869 Lloyd, J. M. , 2006. Modern distribution of benthic foraminifera from Disko Bugt, West
870 Greenland. *Journal of Foraminiferal Research* 36, 315–331.
- 871
- 872 Lloyd, J.M., Moros, M., Perner, K., Telford, R.J., Kuijpers, A., Jansen, E., et al., 2011.
873 A 100 yr record of ocean temperature control on the stability of Jakobshavn

- 874 Isbrae, West Greenland. *Geology* 39 (9), 867-870. <http://dx.doi.org/10.1130/>
875 G32076.1.
876
- 877 Marcott, S.A., et al., 2011. Ice-shelf collapse from subsurface warming as a trigger for
878 Heinrich events. *PNAS* 108,13415-13419: doi:10.107/pnas.1104772108.
879
- 880 Moon, T., Joughin, I., Smith, B., Howat, I., 2012. 21st-centry evolution of Greenland
881 outlet glacier velocities. *Science* 336 (6081), 576-578: doi: 10.1126/science.1219985.
882
- 883 Nick, F. M., Vieli, A., Howat, I. M., Joughin, I., 2009. Large-scale changes in Greenland
884 outlet glacier dynamics triggered at the terminus. *Nature Geoscience* 394, 110–114.
885
- 886 Ó Cofaigh, C., Andrews, J.T., Jennings, A.E., Dowdeswell, J.A., Hogan, K.A.,
887 Kilfeather, A.A., Sheldon, C., 2013a. Glacimarine lithofacies, provenance and
888 depositional processes on a West Greenland trough-mouth fan. *Journal of Quaternary*
889 *Science* 28. Available at: <http://dx.doi.org/10.1002/jqs.2569>: doi:10.1002/jqs.2569.
890
- 891 Ó Cofaigh, C., Dowdeswell, J.A., Jennings, A.E., Hogan, K.A., Kilfeather, .A, Hiemstra,
892 J.F., et al., 2013b. An extensive and dynamic ice sheet on the West Greenland shelf
893 during the last glacial cycle. *Geology* 41(2): 219–222: doi:10.1130/G33759.1.
894
- 895 Perner, K., Moros, M., Jennings, A., Lloyd, J.M., Knudsen, K.L., 2012. Holocene
896 palaeoceanographic evolution off West Greenland. *The Holocene* 23, 374-387.

897

898 Polyak, L., Korsun, S., Febo, L. A., Stanovoy, V., Khusid, T., Hald, M., Paulsen, B. E.,
899 Lubinski, D. J. 2002. Benthic foraminiferal assemblages from the southern Kara Sea, a
900 river-influenced arctic marine environment. *Journal of Foraminiferal Research* 32, 252–
901 273.

902

903 Polyak, L., Solheim, A. 1994. Late- and postglacial environments in the northern Barents
904 Sea west of Franz Josef Land. *Polar Research* 13, 197–207.

905

906 Ramsey, C.B., Lee, S., 2013. Recent and planned developments of the program OxCal.
907 *Radiocarbon* 55, 720-730.

908

909 Reimer, P.J., Bard, E., Bayliss, A., Beck, J.W., Blackwell, P.G., Ramsey, C.B., Grootes,
910 P.M., Guilderson, T.P., Hafliðason, H., Hajdas, I., Hatté, C., Heaton, T.J., Hoffmann,
911 D.L., Hogg, A.G., Hughen, K.A., Kaiser, K.F., Kromer, B., Manning, S.W., Niu, M.,
912 Reimer, R.W., Richards, D.A., Scott, E.M., Southon, J.R., Staff, R.A., Turney, C.S.M.,
913 van der Plicht, J., 2013. IntCal13 and Marine13 radiocarbon age calibration curves 0-
914 50,000 years cal BP. *Radiocarbon* 55, 1869–1887. [http://dx.doi.org/10.2458/azu_js_rc.](http://dx.doi.org/10.2458/azu_js_rc.55.16947)
915 55.16947.

916

917 Ribergaard, M.H., Olsen, S.M., Mortensen, J., 2008. Oceanographic Investigations off
918 West Greenland 2007. NAFO SCR Doc. 08/3, SCIENTIFIC COUNCIL MEETING –
919 June 2008.

920

921 Rignot, E., Fenty, I., Menemenlis, D., Xu, Y., 2012. Spreading of warm ocean waters
922 around Greenland as a possible cause for glacier acceleration. *Annals of Glaciology*
923 53(60). doi: 10.3189/2012AoG60A136

924

925 Rignot, E., Fenty, I., Xu, Y., Cai, C., Kemp, C., 2015. Under-cutting of marine-
926 terminating glaciers in West Greenland, *Geophys. Res. Lett.* 42, 5909–5917,
927 doi:10.1002/2015GL064236.

928

929 Rignot, E., Mouginot, J., 2012. Ice flow in Greenland for the International Polar Year
930 2008-2009. *Geophysical Research Letters* 39, L11501, doi:10.1029/2012GLO51634,
931 2012.

932

933 Roberts, D.H., Rea, B.R., Lane, T.P., Schnabel, C., Rodés, A., 2013. New constraints on
934 Greenland ice sheet dynamics during the last glacial cycle: evidence from the
935 Uummannaq ice stream system. *J. Geophys. Res. Earth Surf.* 118 (2), 519-541.
936 <http://dx.doi.org/10.1002/jgrf.20032>.

937

938 Rytter, F., Knudsen, K. L., Seidenkrantz, M.-S., Eiríksson, J., 2002. Modern distribution
939 of benthic foraminifera on the North Icelandic shelf and slope. *Journal of Foraminiferal*
940 *Research* 32, 217–244.

941

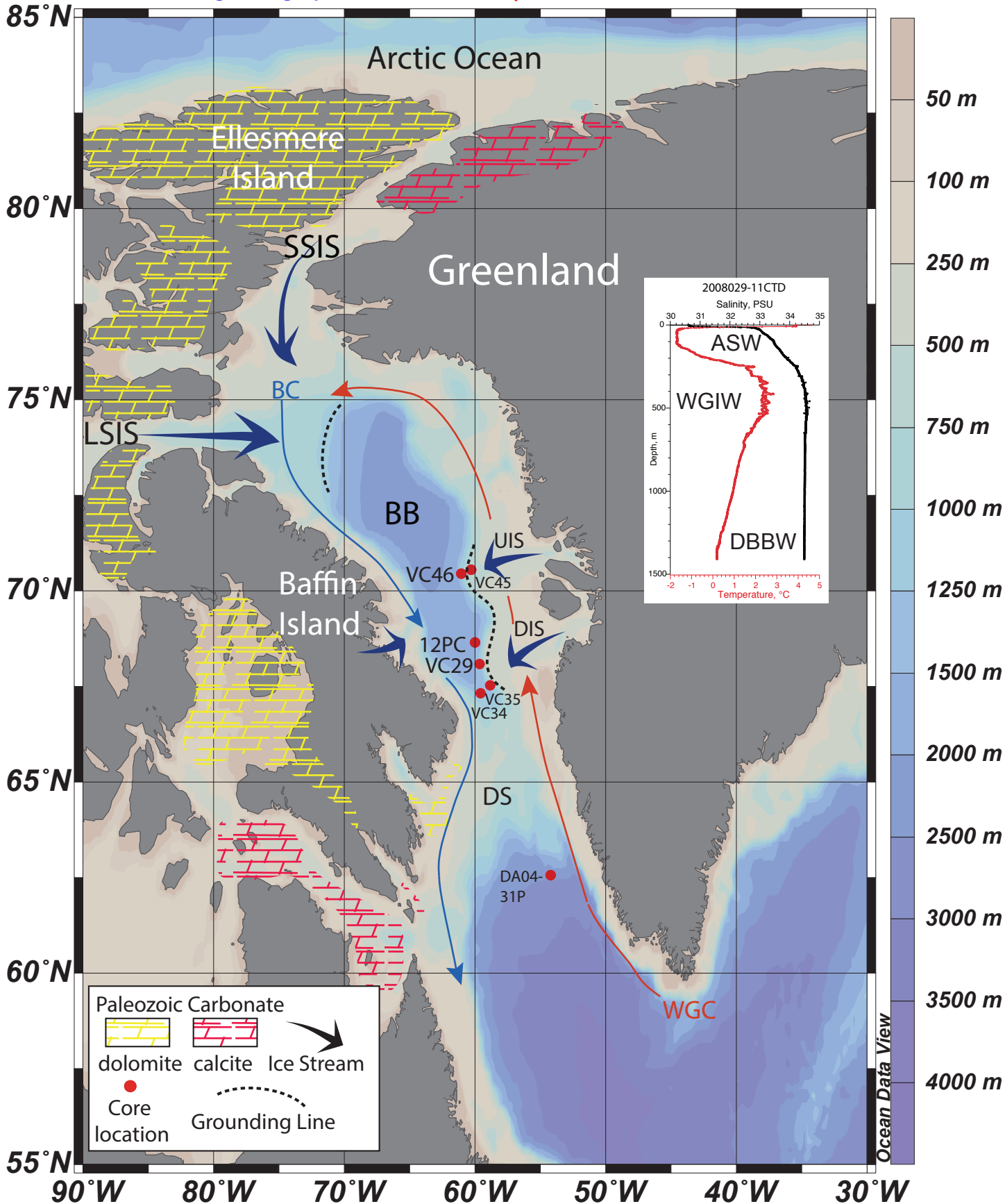
- 942 Schafer, C.T., Cole, F.E., 1986. Reconnaissance survey of benthonic foraminifera from
943 Baffin Island fiord environments. *Arctic* 39, 232-239.
944 <http://dx.doi.org/10.14430/arctic2079>.
945
- 946 Schafer, C.T., Cole, F.E., 1988. Environmental associations of Baffin Island fjord
947 agglutinated foraminifera. *Abh. Geol. Bundesanst*, 307.
948
- 949 Schröder-Adams, C. J., Cole, F. E., Medioli, F. S., Mudie, P. J., Scott, D. B., Dobbin, L.
950 1990. Recent arctic shelf foraminifera: Seasonally ice covered vs. perennially ice covered
951 areas. *Journal of Foraminiferal Research* 20, 8–36.
952
- 953 Scott, D.B., Vilks, G., 1991. Benthic foraminifera in the surface sediments of the deepsea
954 Arctic ocean. *Journal of Foraminiferal Research* 21, 20-38. [http://dx.doi.org/10.2113/
955 gsjfr.21.1.20](http://dx.doi.org/10.2113/gsjfr.21.1.20).
956
- 957 Seidenkrantz, M.-S., 1995. *Cassidulina teretis* Tappan and *Cassidulina neoteretis* new
958 species (Foraminifera): stratigraphic markers for deep sea and outer shelf areas. *J.*
959 *Micropalaeontology* 14, 145-157. <http://dx.doi.org/10.1144/jm.14.2.145>.
960
- 961 Seidenkrantz, M.-S., 2013. Benthic foraminifera as palaeo sea-ice indicators in the
962 subarctic realm-examples from the Labrador Sea-Baffin Bay region. *Quaternary Science*
963 *Reviews* 79, 135-144. <http://dx.doi.org/10.1016/j.quascirev.2013.03.014>
964

- 965 Sheldon, C., Jennings, A., Andrews, J.T., Ó Cofaigh, C., Hogan, K., Dowdeswell, J.A.,
966 Seidenkrantz, M-S., 2016. Ice stream retreat following the LGM and onset of the west
967 Greenland current in Ummannaq Trough, west Greenland. *Quaternary Science Reviews*,
968 <http://dx.doi.org/10.1016/j.quascirev.2016.01.019>
969
- 970 Simon, Q., Hillaire-Marcel, C., St-Onge, G., Andrews, J.T., 2014. Northeastern
971 Laurentide, western Greenland and southern Inuitian ice stream dynamics during the last
972 glacial cycle. *Journal of Quaternary Science* 29(1): 14-26. DOI: 10.1002/jqs.2648
973
- 974 Slubowska, M.A., Koç, N., Rasmussen, T.L., Klitgaard-Kristensen, D., 2005. Changes in
975 the flow of Atlantic water into the Arctic Ocean since the last deglaciation: evidence from
976 the northern Svalbard continental margin, 80°N. *Paleoceanography* 20, PA4014.
977 doi:10.1029/2005PA001141.
978
- 979 Steinsund, P. I., 1994. Benthic Foraminifera in Surface Sediments of the Barents and
980 Kara Seas: Modern and Late Quaternary Applications. Ph.D. dissertation, University of
981 Tromsø, 111 pp.
982
- 983 Straneo, F., Heimbach, P., 2013. North Atlantic warming and the retreat of Greenland's
984 outlet glaciers. *Nature* 504, 36–43, doi:10.1038/nature12854.
985
- 986 Straneo, F., Sutherland, D.A., Holland, D., Gladish, C., Hamilton, G.S., Johnson, H.L.,
987 Rignot, E., Xu, Y., Koppes, M., 2012. Characteristics of ocean waters reaching

- 988 Greenland’s glaciers. *Annals of Glaciology* 53(60), 202-210.
989 doi:10.3189/2012AoG60A059
990
- 991 Tang, C.C.L., Ross, C.K., Yao, T., Petrie, B., DeTracey, B.M., Dunlap, E., 2004. The
992 circulation, water masses and sea-ice of Baffin Bay. *Progress in Oceanography* 63, 183–
993 228.
994
- 995 Vasskog, K., Langebroek, P.M., Andrews, J.T., Nilsen, J.E.Ø., Nesje, A., 2015. The
996 Greenland Ice Sheet during the last glacial cycle: Current ice loss and contribution to sea-
997 level rise from a palaeoclimatic perspective. *Earth-Science Reviews* 150, 45-67.
998
- 999 Wollenburg, J. E., Mackensen, A., 1998. Living benthic foraminifera from the central
1000 Arctic Ocean: Faunal composition, standing stock and diversity. *Marine*
1001 *Micropaleontology* 34, 153–185.
1002
- 1003 Wollenburg, J.E., Knies, J., Mackensen, A., 2004. High-resolution paleoproductivity
1004 fluctuations during the past 24 kyr as indicated by benthic foraminifera in the
1005 marginal Arctic Ocean. *Palaeogeography, Palaeoclimatology, Palaeoecology* 204, 209-
1006 238.
1007
- 1008 Zreda, M., England, J., Phillips, F., Elmore, D., Sharma, P., 1999. Unblocking of the
1009 Nares Strait by Greenland and Ellesmere Ice-Sheet retreat 10,000 years ago. *Nature*
1010 398,139–142, <http://dx.doi.org/10.1038/18197>

"Disclaimer: This is a pre-publication version. Readers are recommended to consult the full published version for accuracy and citation."

Figure
[Click here to download Figure: Fig.1.pdf](#)



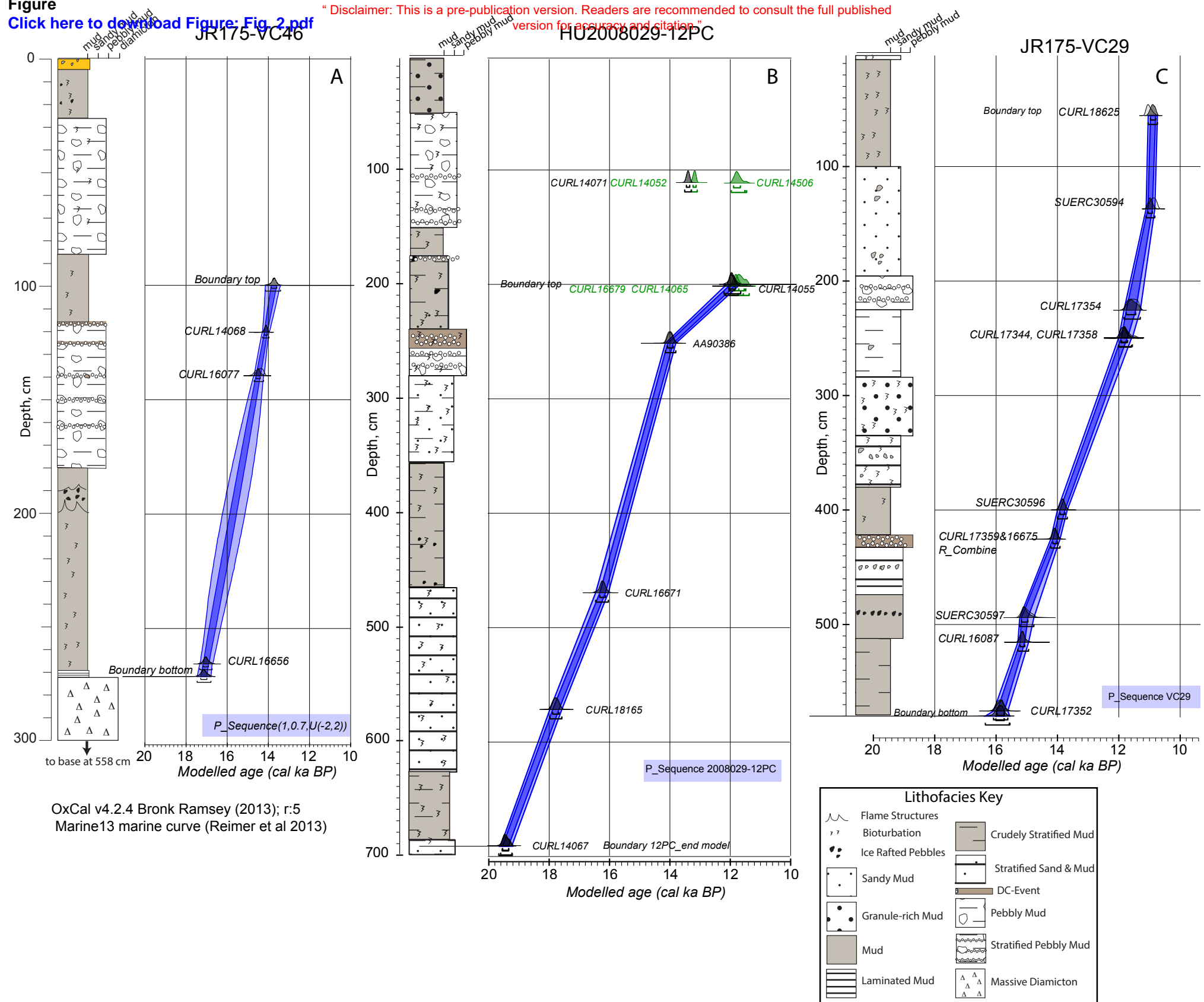


Figure 3 “Disclaimer: This is a pre-publication version. Readers are recommended to consult the full published version for accuracy and citation.”

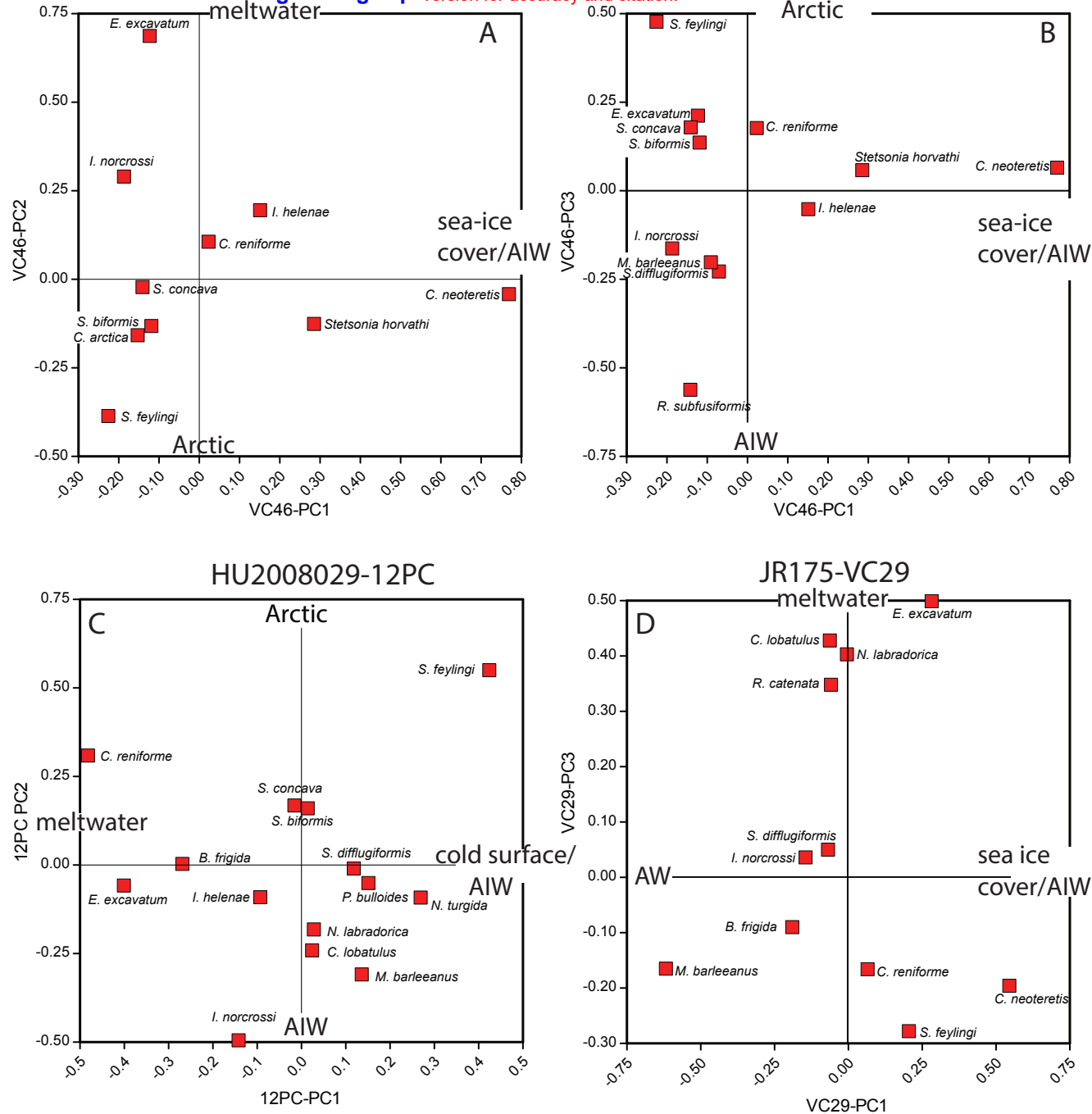
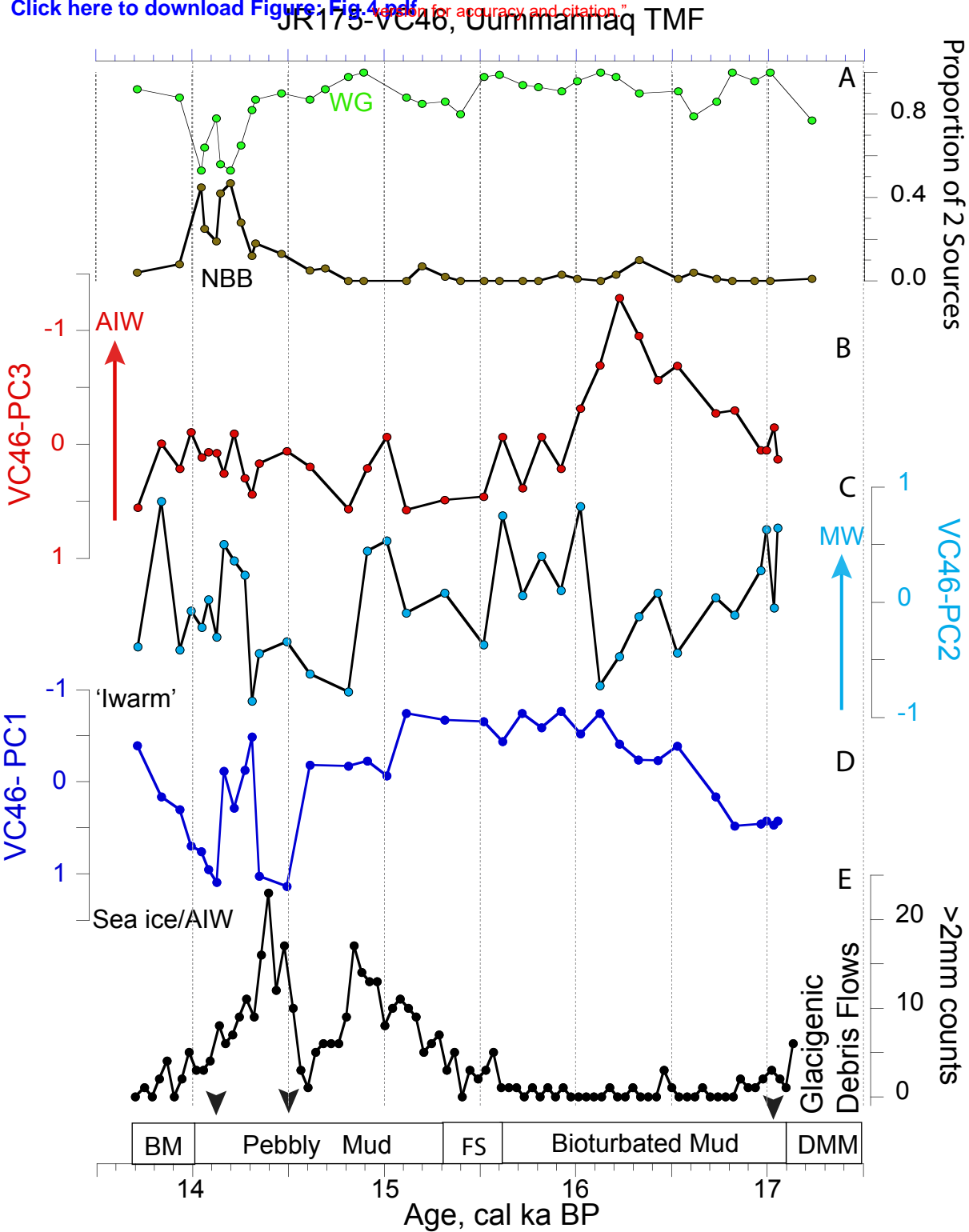


Figure "Disclaimer: This is a pre-publication version. Readers are recommended to consult the full published [Click here to download Figure: Fig. 4.pdf](#) for accuracy and citation"



2008029-12PC Northern Disko TME

Disclaimer: This is a pre-publication version. Readers are encouraged to consult the full published version for accuracy and citation.

Click here to download Figure 5.pdf

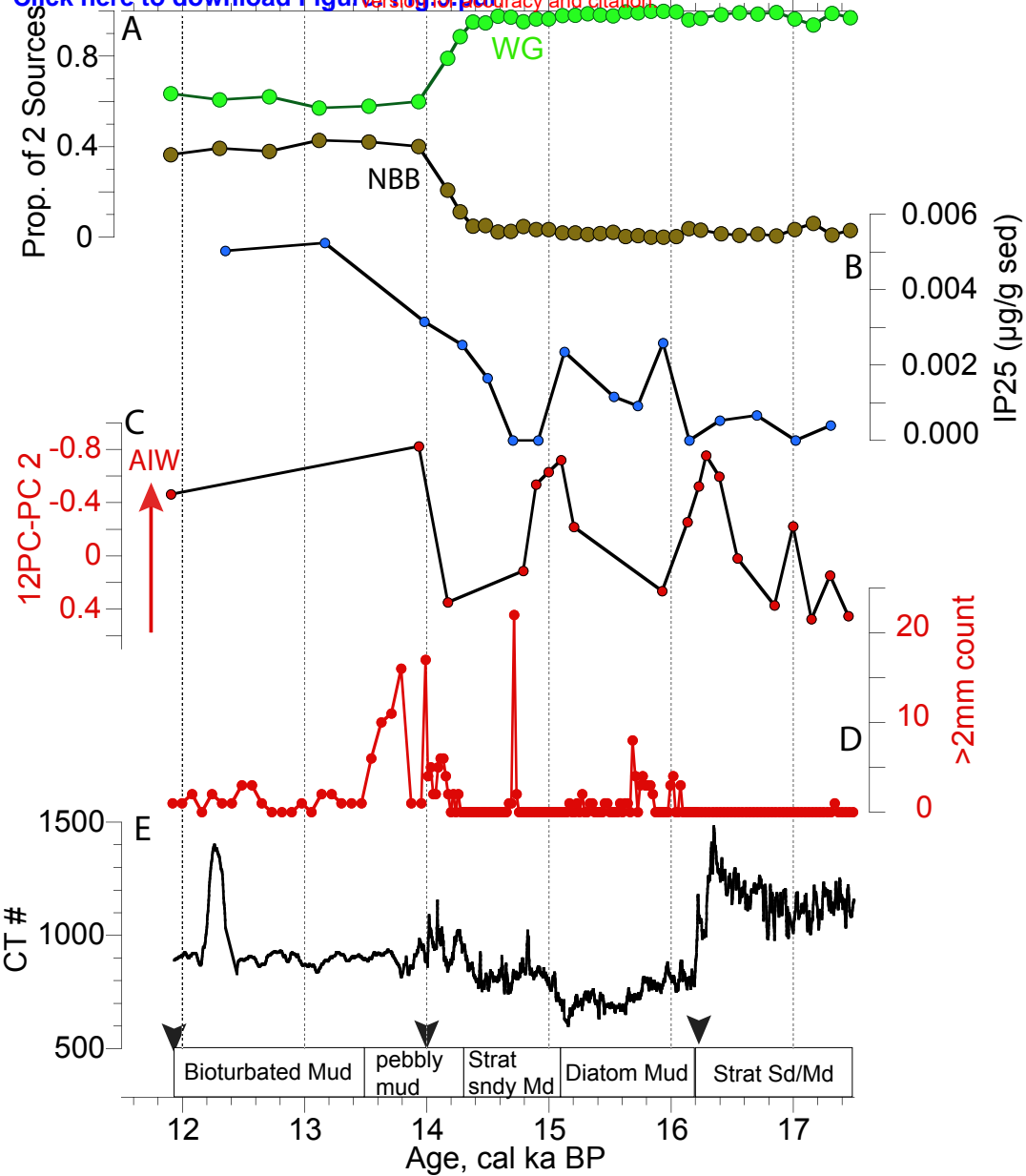
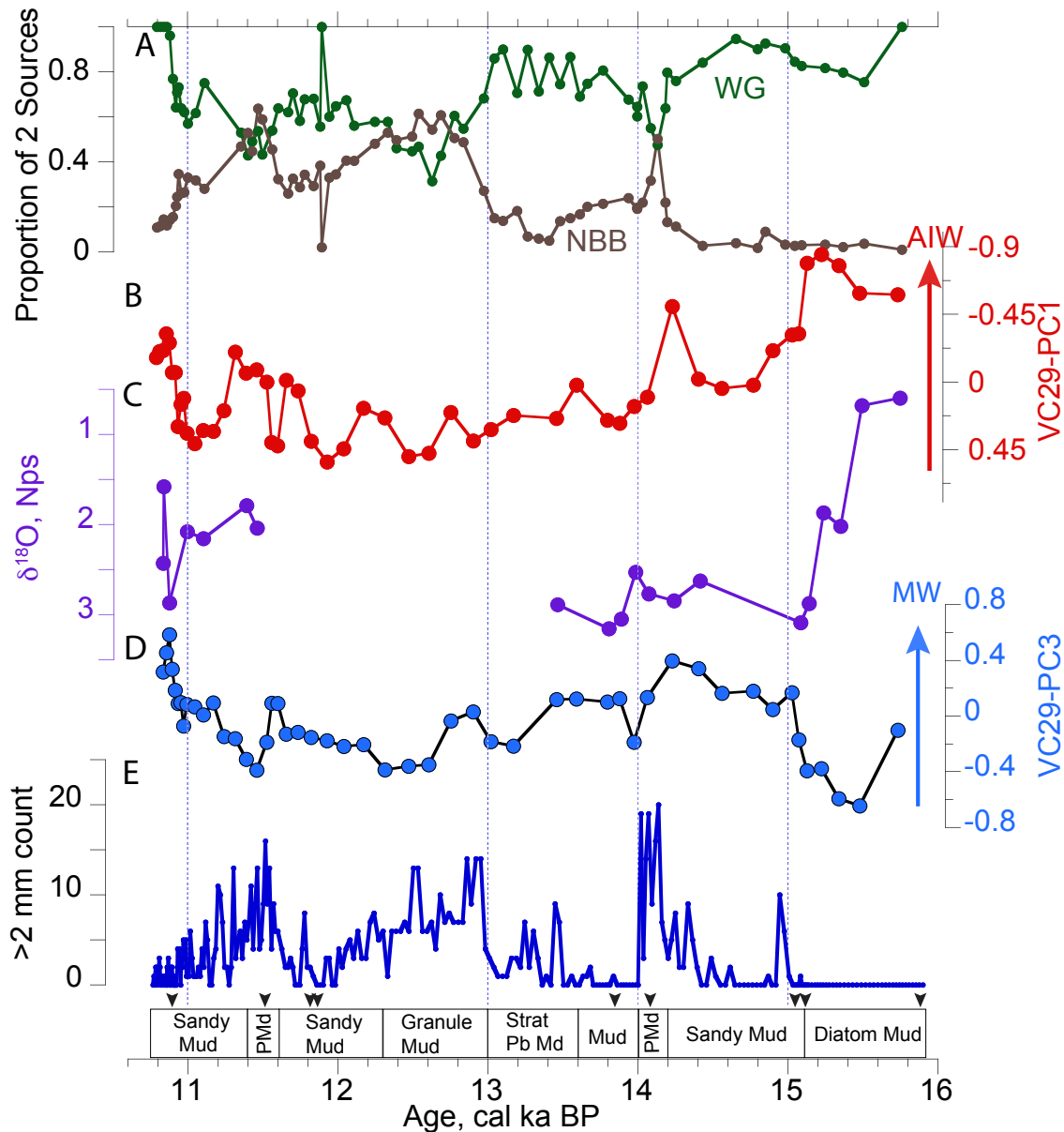
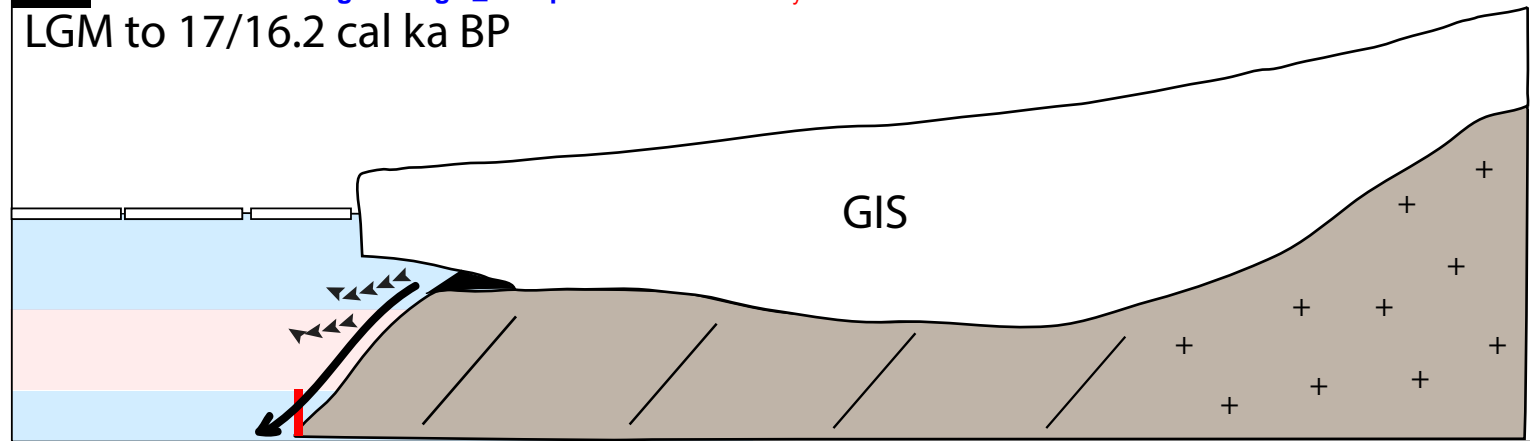


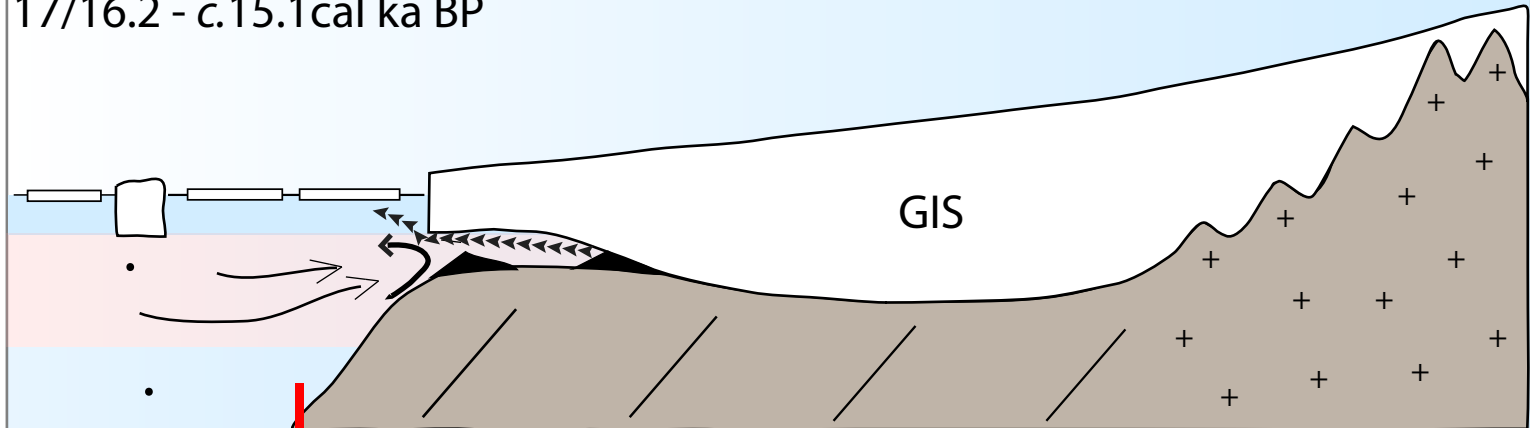
Figure 4 [†]Disclaimer: This is a pre-publication version. Readers are recommended to consult the full published version of this article. [Click here to download Figure 4](#) (1.8 MB) or [Figure 4](#) (1.8 MB) (PDF) and [Figure 4](#) (1.8 MB) (TIFF)



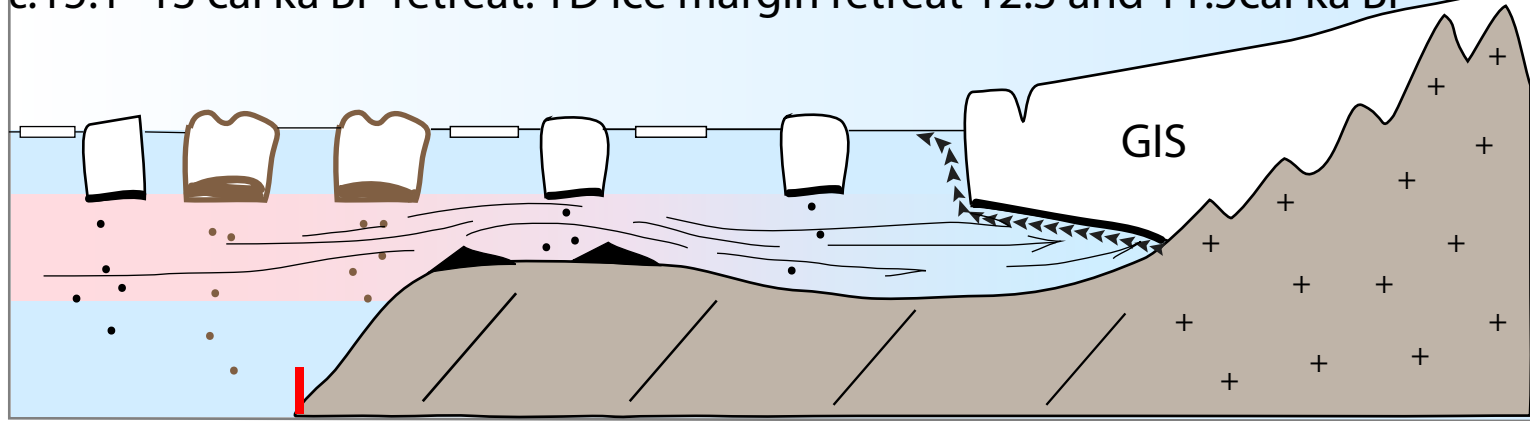
A [Click here to download Figure: Fig.7_rev2.pdf](#)
LGM to 17/16.2 cal ka BP



B
17/16.2 - c.15.1 cal ka BP



C
c.15.1 - 13 cal ka BP retreat. YD ice margin retreat 12.3 and 11.5 cal ka BP



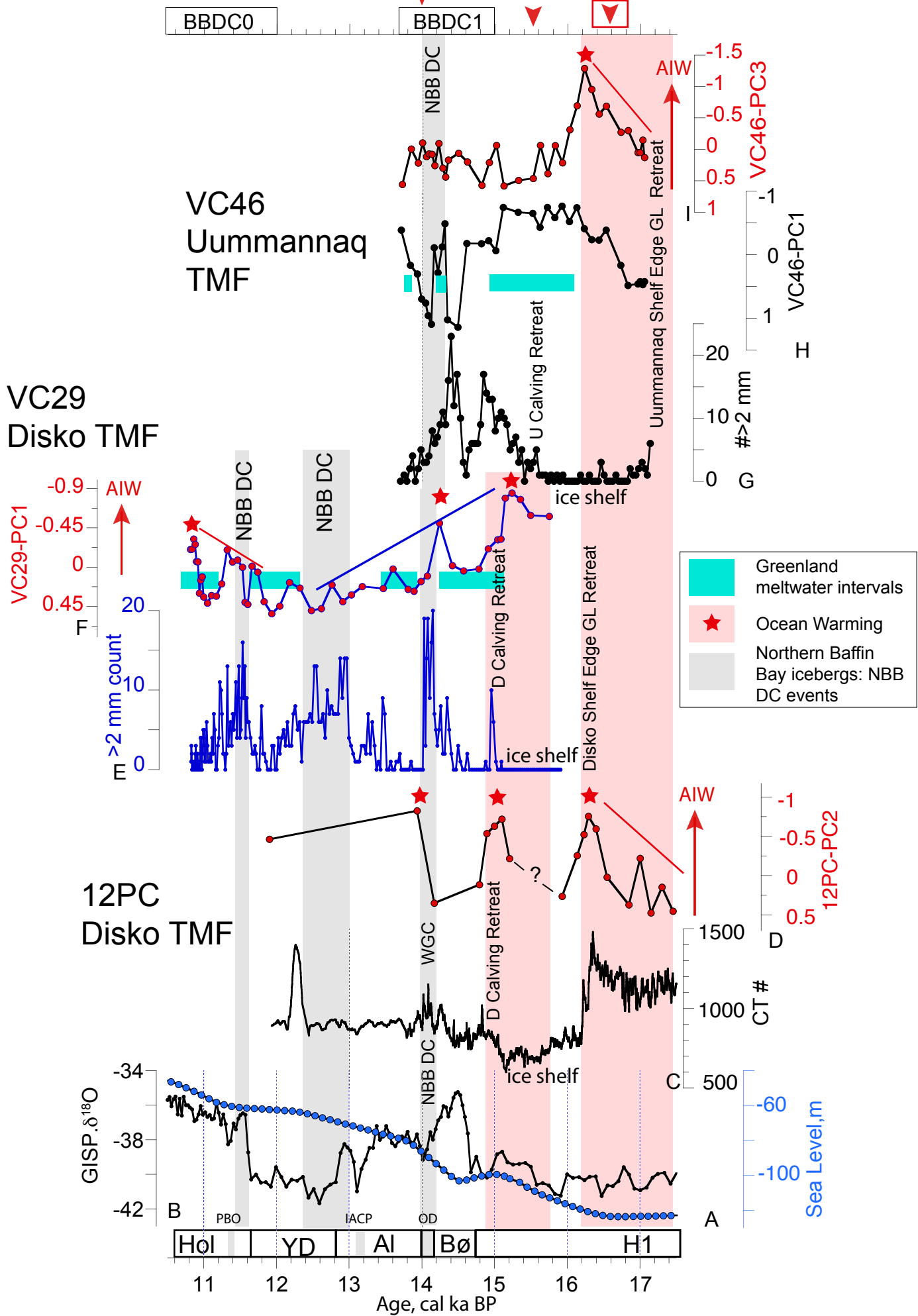


Table 1. Central West Greenland Radiocarbon Dates

Core Name	Reported Age	Reported Uncertainty	Radio-carbon Lab	Radio-carbon Lab Number	$\delta^{13}\text{C}$	Depth, cm	Material Dated	Sample Weight, mg	Calibrated ages, unmodelled (BP)								
									1sigma			2sigma					
									from	to	%	from	to	%	μ	σ	m
JR175-VC46	12770	30	CURL	14068	-0.3	120-121	<i>Cassidulina neoteretis</i>	4.5	14187	14045	68.2	14276	13961	95.5	14121	78	14118
JR175-VC46	12930	40	CURL	16077	3.1	139-140	Echinoid	7.6	14600	14236	68.2	14776	14141	95.5	14450	172	14435
JR175-VC46	14570	60	CURL	16656	4.7	262-267	NPS	2.3	17174	16915	68.2	17328	16749	95.5	17035	137	17070
HU2008029-012PC	11955	40	CURL	14071	5.8	110-112	NPS	2.3	13453	13344	68.2	13509	13295	95.4	13401	54	13400
HU2008029-012PC	10760	35	CURL	14065	4.8	201-202	NPS	1.2	12037	11845	68.2	12155	11715	95.4	11935	101	11942
HU2008029-012PC	12666	61	AA	90386	0.4	251-252	NPS	8.3	14100	13920	68.2	14177	13826	95.4	14007	88	13976
HU2008029-012PC	14030	40	CURL	16671	-1	469-470	NPS	6.6	16320	16133	68.2	16450	16033	95.4	16233	98	16225
HU2008029-012PC	15150	60	CURL	18165	-0.6	571-572	NPS	4.8	17891	17681	68.2	17980	17586	95.4	17784	100	17771
HU2008029-012PC	16660	45	CURL	14067	1	690-691	NPS	8.4	19555	19360	68.2	19619	19246	95.4	19446	76	19308
HU2008029-012PC	16600	50	CURL	16663	-1.1	780-781	NPS	5.5	19485	19275	68.2	19570	19187	95.4	19378	75	19500
HU2008029-012PC	18540	80	CURL	18628	0.2	859-860	NPS	5	21920	21661	68.2	22070	21525	95.4	21795	131	21758
HU2008029-012PC	11690	30	CURL	14052	2.1	110-112	<i>Cassidulina neoteretis</i>	3.9	13233	13132	68.2	13284	13095	95.4	13186	49	13185
HU2008029-012PC	10525	30	CURL	14506	-0.1	111-112	<i>Cassidulina neoteretis</i>	4.5	11890	11666	68.2	11963	11459	95.4	11749	123	11767
HU2008029-012PC	10490	40	CURL	16679	0.2	201-202	<i>Cassidulina neoteretis</i>	5.2	11829	11479	68.2	11904	11374	95.4	11653	142	11667
HU2008029-012PC	10540	25	CURL	14055	-1.3	201-202	<i>Cassidulina neoteretis</i>	5.4	11909	11720	68.2	11994	11568	95.4	11792	106	11804
JR175-VC29	10160	40	CURL	18625	4	54-57	Mixed benthic species	82	11115	10941	68.2	11160	10820	95.4	11006	88	11018
JR175-VC29	10057	39	SUERC	30594	-7	137	Paired bivalve	101.8	10975	10774	68.2	11058	10706	95.4	10880	93	10878
JR175-VC29	10570	40	CURL	17354	0.1	225-226	Mixed benthic species	4.4	11675	11370	68.2	11807	11281	95.4	11542	142	11538
JR175-VC29	10690	40	CURL	17344	-0.9	249-250	2 small gastropods	5.5	11962	11700	68.2	12025	11456	95.4	11788	143	11809
JR175-VC29	10710	35	CURL	17358	0.3	249-251	<i>Cassidulina neoteretis</i>	5.5	11980	11758	68.2	12065	11552	95.4	11837	125	11853
JR175-VC29	12494	41	SUERC	30596	0.3	400	Paired bivalve	4.1	13906	13753	68.2	13990	13674	95.4	13831	78	13830
JR175-VC29	12805*	50	CURL	17359	0.3	424-427	<i>Cassidulina neoteretis</i>	5.3	14132	13978	68.2	14205	13885	95.4	14052	80	14053
JR175-VC29	12710*	45	CURL	16675	-2.6	425-426	NPS	3.1	14269	14055	68.2	14512	13965	95.4	14200	135	14176
JR175-VC29	13194	63	SUERC	30597	-1.2	494	Paired bivalve	3.7	15189	14905	68.2	15275	14712	95.4	15011	151	15035
JR175-VC29	13255	40	CURL	16087	3.3	515-516	NPS	3.6	15238	15070	68.2	15313	14917	95.4	15134	96	15145
JR175-VC29	13760	60	CURL	17352	0.1	574-577	NPS	4.1	16000	15771	68.2	16111	15662	95.4	15884	114	15884

*mean of 2 dates used in age model

outliers or dates not used in age model

Table 2. Benthic foraminiferal environmental preferences.								
<i>Species</i>	<i>Atlantic Water</i>	<i>Arctic</i>	<i>Productivity</i>	<i>Glacial Meltdown</i>	<i>Seasonal sea ice cover</i>	<i>Sea ice cover, low productivity</i>	<i>Strong currents</i>	<i>References</i>
Calcareous Species								
<i>Astrononion gallowayi</i>						X		Polyak et al., 2002
<i>Buccella frigida</i>	X		X		X			Polyak and Solheim, 1994; Steinsund, 1994
<i>Cassidulina neoteretis</i>	X				X			Jennings and Helgadottir, 1994; Seidenkrantz, 1995
<i>Cassidulina reniforme</i>	X			X	X			Hald and Korsun, 1997; Slubowska et al., 2005
<i>Cibicides lobatulus</i>							X	Wollenburg and Mackensen, 1998; Korsun and Polyak, 1989
<i>Elphidium excavatum</i> f. <i>clavata</i>		X		X				Hald and Korsun, 1997; Jennings and Helgadottir, 1994
<i>Epistominella arctica</i>		X				X		Wollenburg and Mackensen, 1998
<i>Islandiella helenae</i>		X	X		X			Wollenburg et al., 2004
<i>Islandiella norcrossi</i>	X				X			Lloyd, 2006; Steinsund, 1994; Korsun and Hald, 1998
<i>Melonis barleeanus</i>	X		X		X			Caralp, 1989; Corliss, 1991; Jennings et al., 2004; Wollenburg and Mackensen, 1998
<i>Nonionella turgida</i>	X		X		X			Wollenburg et al., 2004; Jennings et al., 2004; Rytter et al., 2002
<i>Nonionellina labradorica</i>			X		X			Jennings et al., 2004; Polyak et al., 2002; Rytter et al., 2002
<i>Pullenia bulloides</i>	X							Wollenburg et al., 2004; Rytter et al., 2002
<i>Stainforthia concava</i>		X	X		X			Steinsund, 1994; Jennings and Helgadottir, 1994; Polyak et al., 2002
<i>Stainforthia feylingi</i>		X	X		X			Knudsen and Seidenkrantz, 1994; Seidenkrantz, 2013
<i>Stetsonia horvathi</i>		X				X		Wollenburg and Mackensen, 1998
Agglutinated Species								
<i>Cuneata arctica</i>		X						Schafer and Cole, 1988; Lloyd, 2006
<i>Portatrochammina bipolaris</i>		X						Jennings and Helgadottir, 1994; Schröder-Adams et al., 1990
<i>Reophax catella</i>	X							Höglund, 1947
<i>Reophax catenata</i>	X							Höglund, 1947
<i>Reophax subfusiformis</i>	X							Lloyd, 2006 (as <i>R. fusiformis</i>)
<i>Saccammina difflugiformis</i>	X							Schafer and Cole, 1988; Scott and Vilks, 1991
<i>Spiroplectammina biformis</i>		X		X				Jennings and Helgadottir, 1994; Schafer and Cole, 1986
<i>Textularia earlandi</i>	X	X						Jennings and Helgadottir, 1994; Schafer and Cole, 1986; Lloyd, 2006